REVIEW ARTICLE

Superhydrophobic Surface for Ice Mitigation: Mechanisms, Fabrication Strategies, and Applications

Jingxian Yang[1], **Zhangyu Wu**[2,*], **Binbin He**[1,*] **and Wei She**[2]

[1] Faculty of Environmental Science and Engineering, Kunming University of Science and Technology, Kunming 650500, China
[2] State Key Laboratory of Engineering Materials for Major Infrastructure, School of Materials Science and Engineering, Southeast University, Nanjing 211189, China

Abstract

Superhydrophobic surfaces (SHS), characterized by low surface energy and minimal adhesion to liquids, have attracted extensive attention for applications such as self-cleaning, waterproofing, dust resistance, and corrosion protection. Beyond these traditional functions, the de-icing and anti-icing capabilities of SHS have recently garnered significant interest due to their inherent passive ice-shedding behavior. However, a comprehensive, mechanistic understanding of icing phenomena on SHS, along with effective strategies for improving ice-phobic performance, remains inadequately established. This review presents a systematic evaluation of passive and hybrid active–passive anti-icing and de-icing mechanisms, clarifying the theoretical principles underlying interfacial wetting, nucleation, solidification, and ice adhesion on SHS. It further summarizes recent advances in the design and fabrication of three key categories of SHS-based ice-phobic materials, micro/nanostructured superhydrophobic surfaces, superhydrophobic slippery surfaces, and photothermally responsive superhydrophobic materials—and provides a critical assessment of strategies for enhancing their performance. Finally, the review highlights persistent challenges and emerging opportunities, offering forward-looking perspectives to guide the development of next-generation SHS for robust, durable, and scalable anti-icing and de-icing applications.

Keywords: superhydrophobic surface, de-icing, anti-icing, super-slippery, photothermal.

1 Introduction

Inspired by the lotus leaf, superhydrophobic surface (SHS) exhibit characteristics such as a contact angle (CA) >150° and a sliding angle (SA) <10°, making them a milestone achievement in the field of biomimetic functional materials. Barthlott [1] and Neinhuis [2] discovered that the "superhydrophobic effect" of the lotus leaf results from the synergistic action of micron-scale protrusions and nano-scale wax crystals on its surface. Jiang and colleagues further

Submitted: 29 November 2025
Accepted: 25 December 2025
Published: 26 January 2026

Vol. 2, **No.** 1, 2026.
10.62762/JAMR.2025.980268

***Corresponding authors:**
✉ Zhangyu Wu
wuzy@seu.edu.cn
✉ Binbin He
Kust2024hb@163.com

Citation
Yang, J., Wu, Z., He, B., & She, W. (2026). Superhydrophobic Surface for Ice Mitigation: Mechanisms, Fabrication Strategies, and Applications. *Journal of Advanced Materials Research*, 2(1), 14–39.

© 2026 by the Authors. Published by Institute of Central Computation and Knowledge. This is an open access article under the CC BY license (https://creativecommons.org/licenses/by/4.0/).

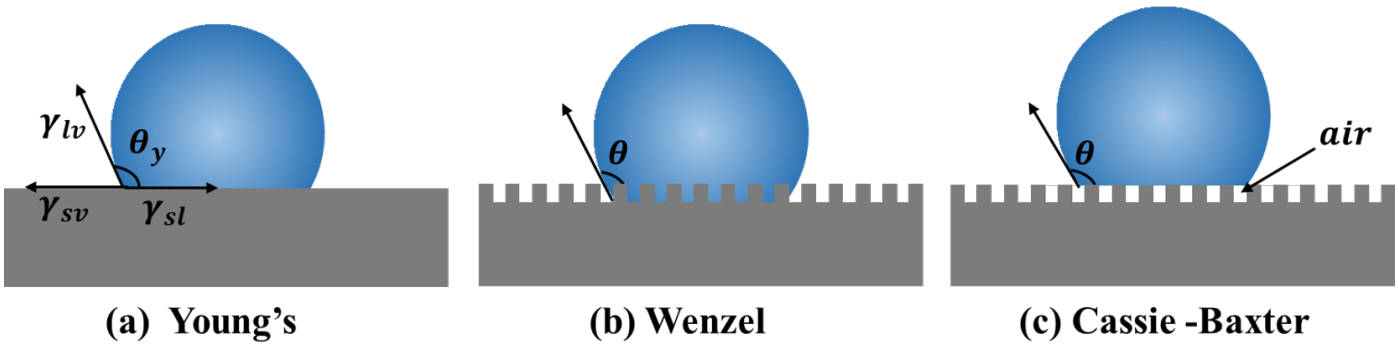


Figure 1. Solid surface wettability model. (a) Young's theoretical model. (b) Wenzel's theoretical model. (c) Cassie-Baxter theoretical model.

refined the SHS theoretical framework, revealing the presence of nanoscale flocs on the surface's micron-scale protrusions [3–5]. This "micron-nano" dual-scale hierarchical structure is the fundamental reason for achieving surface superhydrophobicity. Since then, through biomimicry and replication of such well-defined micro-nanostructures, along with low surface energy chemical modifications, researchers have developed artificial superhydrophobic systems. These systems demonstrate outstanding water-repellent performance and are gradually expanding into practical applications.

In 1805, Young first introduced the concept of surface wettability through thermodynamic equilibrium analysis [6]. The contact angle, as a fundamental parameter, is used to quantitatively describe how a liquid wets a solid surface. Young's equation establishes a quantitative relationship between the contact angle and the interfacial tensions at the solid–liquid–vapor interfaces, as shown in Equation (1) and Figure 1(a):

$$\cos\theta_y = \frac{\gamma_{sv} - \gamma_{sl}}{\gamma_{lv}} \tag{1}$$

where θ_y is the static contact angle, γ_{sv}, γ_{sl}, γ_{lv} are the interfacial tension of solid-vapor, solid-liquid and liquid-vapor, respectively. It can be found from Equation (1), in the fundamental form of Young's equation, the solid-vapor interfacial tension (γ_{sv}) and liquid-vapor interfacial tension (γ_{lv}) are often approximated as constants for a given solid-liquid system under defined conditions. However, it should be noted that γ_{lv}, in particular, is sensitive to variations in temperature and liquid purity. When the same liquid is used, γ_{lv} can be considered relatively stable; hence, the wettability of a solid surface depends primarily on its surface energy (γ_{sv}), provided other conditions remain unchanged. Furthermore, droplets naturally minimize their surface area and tend to adopt a spherical shape due to the cohesive forces acting within the liquid, while adhesive forces at the solid-liquid interface promote spreading [7]. Therefore, if the adhesive forces at the interface exceed the cohesive forces within the liquid, the liquid spreads effectively over the surface—exhibiting hydrophilic behavior. Conversely, if cohesion dominates, the liquid retains a more spherical shape—exhibiting hydrophobic behavior.

In general, liquids wet solid surfaces with high surface energy more effectively than those with low surface energy. Similarly, a significant mismatch—where the solid's surface free energy is much greater than that of the liquid—favors wetting. Recent studies have shown that the surface tension (or surface free energy) of water is approximately 72.8 mN/m at 20 °C [8]. Therefore, a solid with a surface free energy significantly higher than 72.8 mN/m tends to be hydrophilic, whereas a surface energy significantly lower than this threshold typically indicates hydrophobicity. And the lower the surface free energy of a material, the more hydrophobic it is. However, Young's equation represents an idealized model. Perfectly smooth and chemically homogeneous solid surfaces rarely exist in real-world conditions.

To elucidate the mechanism by which surface morphology affects wettability, the Wenzel model was introduced in 1936 [9, 10]. According to this model, a liquid fully wets the rough solid surface, forming a uniform solid–liquid interface. Since the actual solid–liquid contact area of a rough surface is much larger than that of a smooth surface, a roughness factor r is introduced, leading to the following contact angle

equation (as shown in Equation (2) and Figure 1(b)):

$$\cos\theta_w = \frac{r(\gamma_{sv} - \gamma_{sl})}{\gamma_{lv}} = r\cos\theta_y, \qquad r = \frac{\text{actual contact area}}{\text{apparent project area}} \tag{2}$$

where θ_w is the contact angle for a rough solid surface in the Wenzel model, and r is the roughness factor. The model assumes that the liquid can fully penetrate the surface microstructure ($r > 1$), indicating that surface roughness enhances the intrinsic wettability of the material—hydrophilic surfaces become more hydrophilic, while hydrophobic surfaces exhibit stronger hydrophobicity. However, the Wenzel model is only applicable to homogeneous rough surfaces in thermodynamic equilibrium. For solid surfaces with chemical heterogeneity, the fluctuations in surface roughness create potential energy barriers. When the droplet's vibrational energy is insufficient to overcome this barrier ($r \gg 1$), the droplet fails to spread, and the Wenzel model no longer holds.

To address the limitations of the Wenzel model, the Cassie–Baxter model was proposed by Cassie and Baxter in 1944 [11]. This model assumes that the interface between a liquid and a chemically or structurally heterogeneous solid surface consists of a composite of solid–liquid and air–liquid interfaces. It describes the incomplete wetting state that arises on hydrophobic surface due to air entrapment in Equation (3) and Figure 1(c)):

$$\cos\theta_c = f_a\cos\theta_a + f_s\cos\theta_s \tag{3}$$

where, θ_s is the intrinsic contact angle of the liquid on the solid substrate, $\theta_a = 180^\circ$ is the contact angle of the liquid on air (typically considered), f_s represents the fraction of the projected area that is in contact with the solid surface, and $f_a = 1 - f_s$ is the fraction in contact with air. In reality, the wetting state of a solid surface is not always stable. The Wenzel and Cassie–Baxter states may coexist and dynamically transition between one another. A surface enters the Cassie state only when the surface roughness exceeds a certain critical threshold. In this state, increased surface roughness enhances the stability of the wetting behavior.

Based on the theoretical framework, SHS have broad prospects in various applications such as self-cleaning, corrosion resistance, oil-water separation, and dust prevention, especially in de-icing applications [12–15]. Traditional anti-/de-icing methods, including mechanical vibration strategies, resistive heating techniques, and chemical agents, often lead to excessive energy consumption and environmental pollution [16, 17]. In contrast, SHS exhibit significant advantages and practical value over traditional cleaning technologies. As a typical passive anti-icing material, SHS can prevent water from adhering before ice formation, delay the freezing time, and reduce the adhesion force of ice [18, 19]. However, the fragile micro-nano hierarchical structure of SHS is prone to gradual damage under long-term harsh conditions, which results in the loss of water repellency and ice resistance [20, 21]. Robustness has thus become a key criterion for evaluating the durability of SHS [22]. Moreover, under high temperature and high humidity, as well as low-temperature conditions, complex micro/nano-structures on the surface are easily wetted and mechanically interlocked by ice. The mechanism involves the permeation and subsequent solidification of supercooled water droplets into these surface textures. Upon freezing, the ice forms a solid matrix that anchors itself within the microstructural features, creating a strong mechanical interlock that significantly increases the ice adhesion strength. Therefore, slippery liquid-infused porous surface (SLIPS) technology has been introduced to reduce the adhesion strength of ice and improve anti-icing performance by injecting low surface energy lubricants into porous substrates [23, 24]. However, SLIPS face the inevitable issue of rapid depletion of the limited injected lubricant, leading to exposure and contamination of the internal porous structure, which exacerbates unwanted ice formation [25, 26]. Additionally, since a single passive anti-icing strategy is insufficient to meet practical needs, combining SHS with photothermal functional materials to form multifunctional anti-/de-icing composite materials is also hydrophobic of the coating can prevent some water droplets from adhering to the surface, thus reducing ice crystal formation [27–29]. When irreversible icing occurs, the air gaps in the rough structure hinder heat transfer, delaying the freezing process. Simultaneously, the heat generated by the photothermal effect causes the material surface to heat up quickly, further slowing down the icing process and promoting de-icing [27]. Therefore, a deep understanding of the de-icing and anti-icing mechanisms of various SHS is crucial for the practical application of SHS materials in the de-icing field.

Existing reviews on superhydrophobic surface comprehensively cover several aspects, including

basic superhydrophobic materials, multifunctional superhydrophobic materials, and the diversified applications of superhydrophobic materials. However, there are few articles specifically addressing passive de-icing materials, multifunctional de-icing materials, and the synergistic anti-icing strategies of passive and active de-icing. Moreover, most articles in the de-icing field fail to emphasize the critical role of SHS in both de-icing and anti-icing, and reviews focusing specifically on the unique de-icing and anti-icing mechanisms and performance of SHS are still insufficient. Therefore, in this review, we first introduce the basic surface wettability theory and comprehensively summarize the de-icing and anti-icing mechanisms of SHS. Additionally, we systematically analyze the impact of material structure design regulation on the anti-icing, and discuss synergistic methods that combine SHS with other technologies to enhance their anti-icing performance., aiming to accelerate the practical application and technological breakthroughs of SHS in the de-icing field.

2 De-icing and Anti-icing Mechanisms of Superhydrophobic Surface

In the previous section, it was explained that the realization of superhydrophobicity depends on two key factors: first, low surface energy chemicals, such as fluorosilanes, which have weak interactions with water molecules; and second, a micro-nano hierarchical structure, meaning that the surface of the material must have a rough structure combining both micrometer and nanometer scales. This structure prevents the liquid droplets from fully penetrating the rough surface but instead lifts them up with the help of a significant amount of air, resulting in a composite contact state (Cassie-Baxter state). The Cassie-Baxter state is fundamental to anti-icing ability because it brings about three crucial characteristics: first, an extremely high static contact angle (CA $>150°$), where the water droplet forms almost a perfect spherical shape; second, an extremely small sliding angle (SA $<10°$), where the droplet easily rolls off the surface; and third, a minimal solid-liquid actual contact area, where only about 2-5% of the droplet's bottom makes direct contact with the solid surface, with the remaining area in contact with air. Therefore, superhydrophobicity and the Cassie-Baxter state are the prerequisites for the anti-icing and de-icing mechanisms of SHS.

2.1 Mechanisms of Ice Nucleation and Growth

Understanding the anti-icing properties of superhydrophobic surface requires knowledge of the droplet's icing mechanism. Icing is a complex phenomenon observed both in nature and human activities. Ice formation involves a phase transition, which can occur directly from liquid to solid (freezing), or from vapor to liquid and then to solid (condensation freezing). Regardless of the phase transition pathway, ice formation starts with nucleation. During the icing process, stable ice nucleation occurs when molecular clusters reach a critical size, and further growth leads to the formation of ice crystals [30]. The stability of ice nucleation is essential for ice formation, as no ice crystal can grow without initial nucleation. Therefore, the nucleation rate of ice is a crucial factor in preventing droplet freezing. According to classical nucleation theory, ice nucleation can occur through two mechanisms: homogeneous nucleation and heterogeneous nucleation [31, 32].

Homogeneous nucleation. Under ideal conditions, where the ice nucleation process is unaffected by impurities or external surface, the probability of forming a critical nucleus is uniform throughout the system, a process known as homogeneous nucleation. During icing, a specific group of water molecules naturally aggregate through hydrogen bonding due to thermodynamic forces [33]. As a result of these hydrogen bond interactions, more and more water molecules join together to form small rings. Over time, some of these rings break apart and continually reorganize, with occasional formation of more stable hydrogen bonds at different locations. As this process progresses, the polyhedral structure of the small nucleus gradually develops. The shape and size of the droplets slowly change, evolving into a more stable, lower-energy state that facilitates their transition from liquid to solid. Throughout this process, the formation of new interfaces leads to a decrease in the system's free energy, but the accumulation of ice nuclei increases the free energy at the interface between the ice and the surrounding liquid water. If we assume the crystal embryo is spherical, the overall change in free energy due to the phase transition (the nucleation energy barrier for homogeneous nucleation) can be expressed as the sum of the decrease in volumetric free energy and the increase in surface free energy [34], as shown in the following equation:

$$\Delta G = -\frac{4}{3}\pi r^3 \Delta G_V + 4\pi r^2 \sigma \tag{4}$$

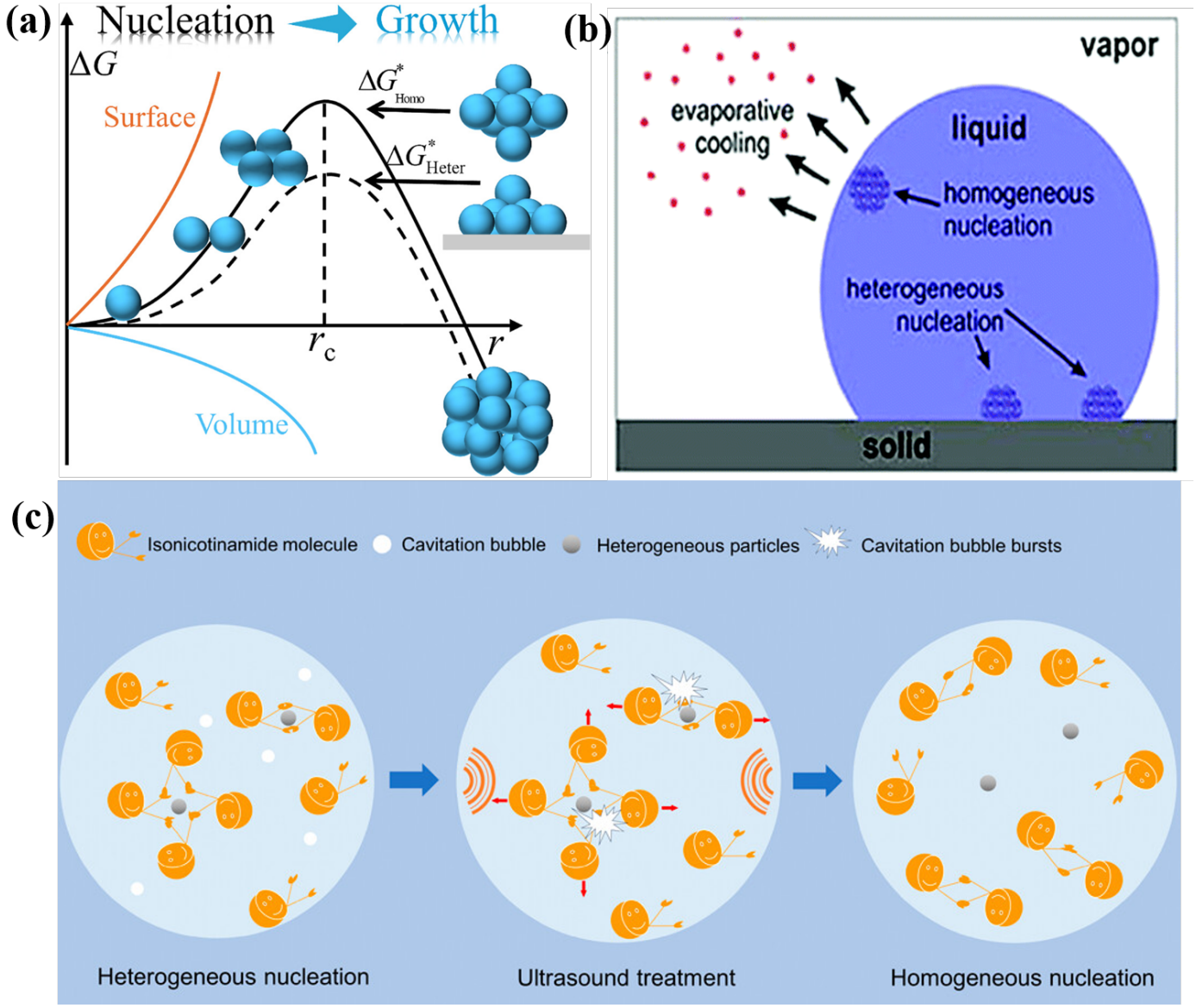


Figure 2. Mechanism diagrams of ice nucleation and growth. (a) Schematic representation of the nucleation barrier as a functional relationship with the nucleation radius [37]. Copyright © 2025 Elsevier B.V. All rights are reserved, including those for text and data mining, AI training, and similar technologies. (b) Schematic depicts the area within a water droplet where the ice may nucleate and potential impacts. Two possible modes of ice nucleation in a water droplet are shown: heterogeneous nucleation and homogeneous nucleation [38]. (c) Regulation from heterogeneous nucleation to homogeneous nucleation [32]. Copyright © 2024 American Chemical Society.

$$\Delta G_V = \frac{\Delta H(T_m - T)}{T_m} \tag{5}$$

where ΔG is the total change in free energy due to the phase transition. r is the radius of the crystal embryo. σ is the specific surface energy, which is expressed by the interfacial tension at the ice-water interface. ΔG_V is the change in volumetric free energy and can be calculated from the Gibbs-Helmholtz equation as shown in Equation (5). ΔH is the volumetric enthalpy of water melting and T_m is the melting temperature of ice.

The total free energy of the system, as depicted in Figure 2(a), results from the balance between the volume free energy and the surface free energy. At a specific temperature, when ΔG reaches its maximum, the ice nucleus radius (r) equals the critical nucleation radius (r_c). This radius, r_c, is known as the critical nucleation radius. For ice nuclei with a radius smaller than r_c, the growth of surface free energy dominates, causing an increase in the system's total free energy. As a result, ice nucleus growth is inhibited at this stage. Only when the ice nucleus radius reaches r_c does ΔG attain its maximum value, which is referred to as the

nucleation energy barrier (ΔG^*).

Beyond this point, the system's free energy begins to decrease, as the reduction in volumetric crystal free energy takes precedence. In other words, once the ice nucleus exceeds the critical radius, stable growth occurs, and nucleation is completed, allowing further crystal growth. The magnitude of the nucleation energy barrier also indicates the ease of nucleation. The critical nucleation radius, as calculated from Equation (6), depends on the degree of subcooling. A higher degree of subcooling leads to a smaller critical nucleation radius. This reduction in the critical radius significantly enhances both the probability of ice nucleation and the number of ice nuclei formed.

$$r_c = \frac{-2\sigma T_m}{\Delta H(T_m - T)} \tag{6}$$

Heterogeneous nucleation. In practice, foreign matter often facilitates nucleation by reducing the free energy of the interface, thereby lowering the nucleation potential barrier [35]. As a result, nucleation tends to occur preferentially at or near the foreign particles, a process known as heterogeneous nucleation. During the freezing of liquid droplets, the presence of foreign matter lowers the nucleation potential barrier, accelerating ice formation (Figure 2(b) and (c)). The nucleation potential for heterogeneous nucleation is lower than that for homogeneous nucleation, and this relationship is well described by equation (7) [36].

$$\Delta G^*_{\text{Heter}} = \Delta G^*_{\text{Homo}} f(r, \theta) \tag{7}$$

where $\Delta G^*_{\text{Heter}}$ and ΔG^*_{Homo} represent the heterogeneous and homogeneous nuclear energy barriers, respectively. The $f(r, \theta)$ represents the static contact angle θ as a function of surface roughness r.

From equation (6) and (7), it can be inferred that superhydrophobic surfaces with large contact angles (greater than $150°$, and even approaching $180°$) exhibit much higher nucleation barriers compared to hydrophilic surfaces, which may even approach the barriers for homogeneous nucleation. Additionally, the limited contact area between the droplet and the superhydrophobic surface, along with an air layer trapped by the micro-nano structures, reduces heat transfer between the surface and the liquid droplets, significantly enhancing the anti-icing performance of the superhydrophobic surface [37].

Furthermore, ice nucleation rate is a key factor affecting the formation of ice nuclei. In classical nucleation theory, the nucleation rate $J(T)$ can be defined as Equation (8) [39]:

$$\tau_{av}^{-1} = J(T) = Ke^{(-\frac{\Delta G^*}{k_B T})} \tag{8}$$

where K is the kinetic constant and k_B is the Boltzmann's constant. The kinetic constant ($K = Z\beta N$) depends on the number of nucleation sites per unit volume of atoms (N), the nonequilibrium factor (Z), and the rate at which atoms or molecules join the critical nucleus (β). However, the dependence of the kinetic constant K on the material properties remains an unresolved issue. As shown in Equation (7), the value of ΔG^* is mainly controlled by the function $f(r, \theta)$, which is a surface ratio. Therefore, the fundamental tuning of the nucleation rate is required in terms of surface energy and micro-nano structures [40]. Relevant results indicate that the kinetics of ice formation depend on surface chemistry, wettability, and morphology [41]. Superhydrophobic surfaces, due to their extremely low solid-liquid contact area, can significantly reduce the nucleation rate at the solid-liquid interface [42]. Additionally, surface temperature is an important factor influencing the nucleation rate [43].

Within the classical theoretical framework of ice nucleation and growth, homogeneous and heterogeneous nucleation represent two fundamentally distinct physical mechanisms. Homogeneous nucleation occurs within the bulk supercooled liquid, requiring the overcoming of a high free-energy barrier, and thus typically demands a substantial degree of supercooling [33]. It is only observable under highly purified, ideal conditions. In contrast, heterogeneous nucleation dominates in natural and engineered environments, where solid surfaces, impurities, or interfaces act as nucleation sites, significantly lowering the energy barrier and enabling ice formation at much higher temperatures [37]. Consequently, surface properties—such as chemical composition, roughness, and surface energy—become key factors in regulating the ice nucleation process [38]. Therefore, the design of modern anti-icing materials is essentially aimed at intervening in heterogeneous nucleation pathways, using engineered surfaces to suppress or delay the generation and attachment of ice nuclei, thereby achieving efficient and low-energy active and passive anti-icing technologies.

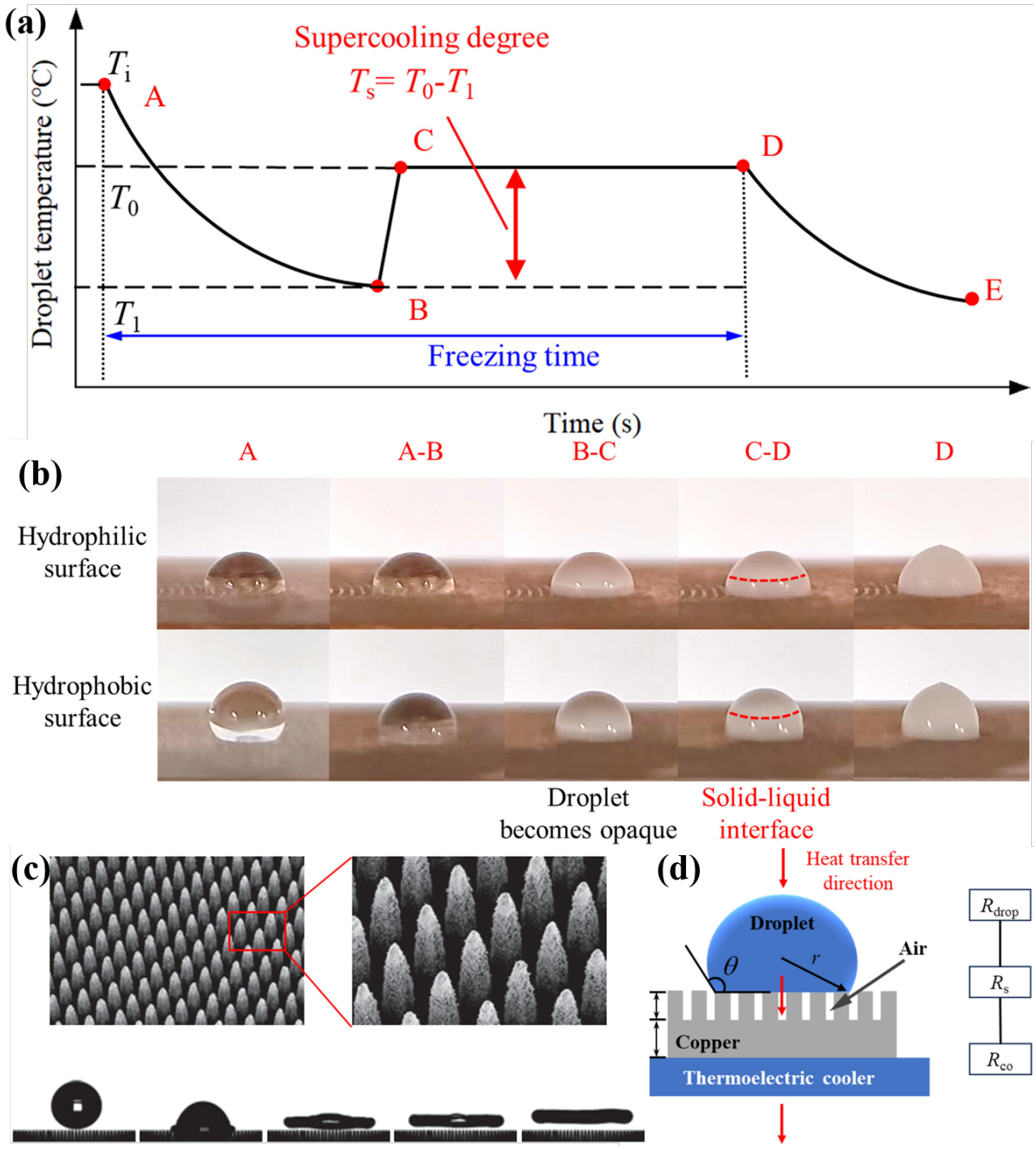


Figure 3. Mechanism Diagrams of anti-icing on SHS. (a) Cooling curve including the four stages of freezing: A-B is the supercooling stage, B-C is the recrystallization stage, C-D is the solidification stage, and D-E is the cooling stage [45] Copyright © 2015 WILEY – VCH Verlag GmbH & Co. kGaA. Weinheim. (b) The freezing process of droplet corresponding to the cooling curve [45]. Copyright © 2015 WILEY – VCH Verlag GmbH & Co. kGaA. Weinheim. (c) The phenomenon of pancake bouncing occurring on the surface of array structures [46] Copyright © 2014, Springer Nature Limited. (d) Schematic diagram of heat transfer thermal resistance: the heat is transferred from the droplet through the copper sheet to the surface of the semiconductor refrigeration sheet during the freezing process. There are three types of thermal resistance between the droplet surface and the cold surface, namely the thermal resistance of the droplet Rdrop, the thermal resistance of microstructures Rs, and the thermal resistance of the copper sheet Rco. The total thermal resistance is the sum of the three thermal resistances mentioned above, which can reflect the synergistic effect of wettability and roughness on the heat transfer intensity during droplet freezing process [45]. Copyright © 2015 WILEY – VCH Verlag GmbH & Co. KGaA. Weinheim.

2.2 Mechanisms of Anti-icing on Superhydrophobic Surface

Based on the aforementioned nucleation mechanism, the core of anti-icing lies in delaying the onset of ice formation, specifically prolonging the supercooled state of water droplets and delaying and inhibiting the formation and growth of ice nuclei [44]. Figure 3(a) presents the temperature profile of a water droplet throughout the freezing process, which can be categorized into four distinct stages. The segment A-B represents the supercooling phase, where the droplet cools from its initial temperature T_i to a metastable state conducive to nucleation. Despite its temperature falling below the equilibrium freezing point, the droplet remains in a liquid state. The temperature at which nucleation initiates is denoted as T_1, and the degree of supercooling is quantified by $T_s = T_0 - T_1$, where T_0 is the freezing point. The interval B-C corresponds to the recalescence phase, during which crystal nuclei rapidly form within the droplet, releasing latent heat and causing a sharp temperature increase back to T_0. This stage is transient, typically lasting only a few hundred milliseconds. The solidification phase occurs between points C and D, where the temperature remains constant at the phase transition point T_0 as the droplet undergoes a liquid-to-solid transition. Finally, the segment D-E marks the post-solidification cooling phase, wherein the temperature of the fully frozen droplet continues to decrease due to heat extraction by the cooling substrate. The total duration from A to E defines the complete freezing time, denoted as t. Due to the presence of an air layer, SHS (superhydrophobic surfaces) can be broken down into three aspects:

Reduction of Ice Nucleation Sites. Ice nucleation on solid surfaces typically occurs heterogeneously at defects, crevices, or surface contaminants (Figure 3(b)). On superhydrophobic surface, the actual solid–liquid contact area is significantly minimized, which greatly reduces the density of potential nucleation "hotspots." Consequently, water droplets require substantially lower temperatures (i.e., higher degrees of supercooling) to undergo homogeneous nucleation or to nucleate at the few available contact points. This markedly delays the onset of ice formation.

Promotion of Condensation Droplet Coalescence and Bouncing. In cold and humid environments, atmospheric water vapor condenses into microscale droplets on surface. On superhydrophobic surface, these droplets remain in the Cassie state, where they exhibit high mobility due to minimal surface adhesion. Upon collision, the droplets rapidly coalesce, and the energy released during coalescence is converted into kinetic energy that propels the merged droplet off the surface. This phenomenon, known as "coalescence-induced droplet jumping" (Figure 3(c)), actively removes nascent condensation droplets before they can freeze and act as nuclei for further ice accretion, thereby maintaining a dry and ice-resistant surface.

Evaporative Cooling Effect. Owing to the limited solid–liquid contact area, local pressure at the contact points can become extremely high, which may lead to instantaneous evaporation of a small volume of liquid (Figure 3(d)). This localized evaporation absorbs latent heat, resulting in rapid cooling at the contact sites. Although this lowers the local temperature, it may also generate micro air pockets that further insulate the droplet from the surface, reducing thermal conductivity. In some instances, the combined effects of evaporative cooling and localized insulation contribute to delaying the overall freezing process of the droplet.

2.3 Mechanisms of De-icing on Superhydrophobic Surface

Even if water droplets eventually freeze, removing the ice layer from a SHS is extremely easy. Previous studies have demonstrated that ice layers forming on rigid substrates exhibit a characteristic critical adhesion length. When the length of the ice layer remains below this threshold, failure occurs due to interfacial strength, and the required de-icing force increases proportionally with ice length. Conversely, once the layer exceeds the critical length, detachment is governed by interfacial toughness rather than strength. Importantly, irrespective of the total icing area, the de-icing force tends to plateau at the value associated with this critical length [47, 48]. The de-icing mechanisms of SHS can be described as follows (Figure 4).

Point Contact Minimizes Surface Interaction to Reduce Ice Adhesion. The adhesion between ice and a solid surface is directly proportional to the actual contact area. On superhydrophobic surface, ice crystals anchor solely at the sparse tips of the micro-nanostructures, resulting in a "point contact" mode. This is in stark contrast to the "surface contact" observed on traditional smooth surface or in the Wenzel state, where the liquid fully wets the rough surface. As a result, the ice adhesion strength is

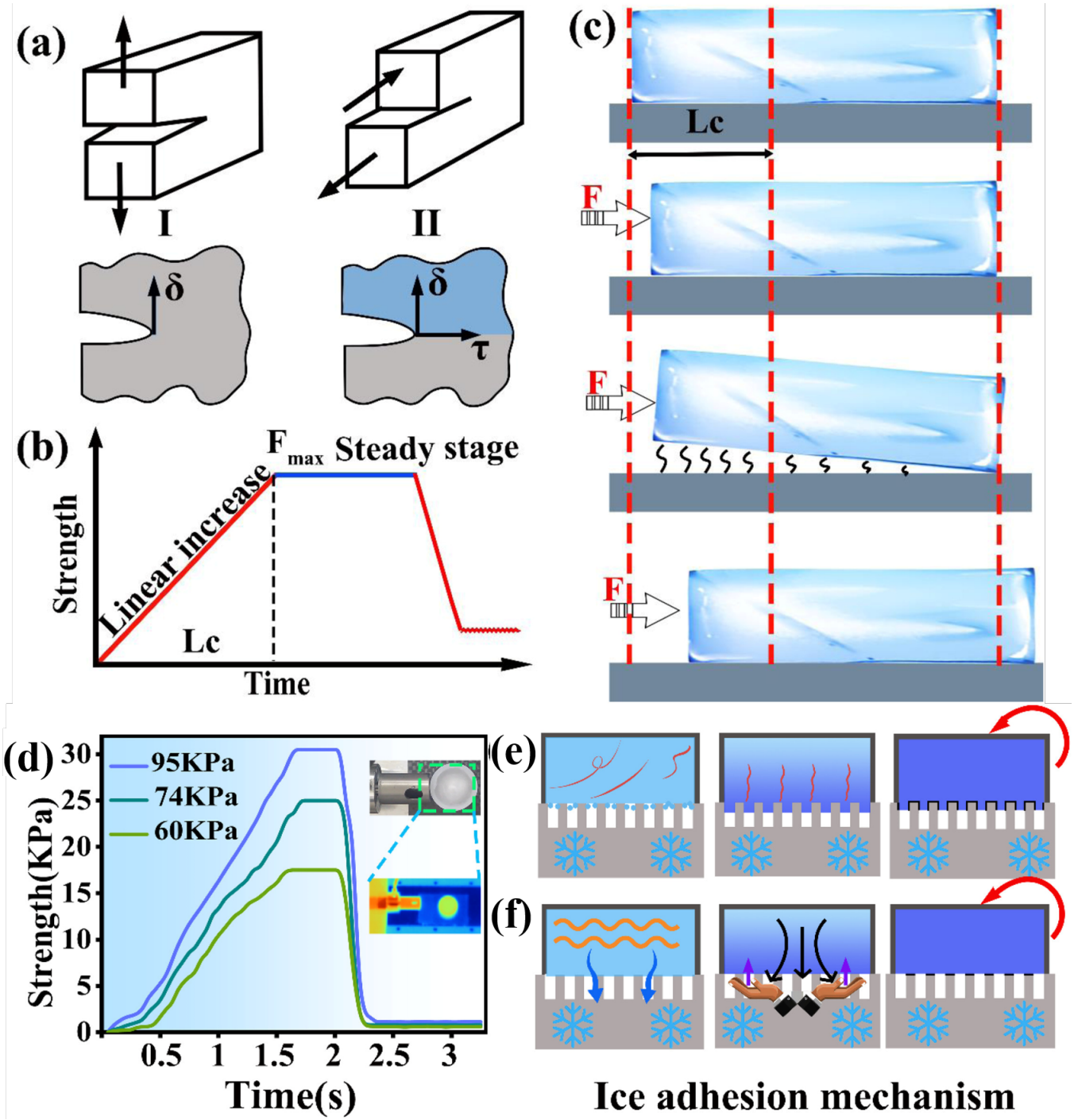


Figure 4. Ice shedding modes on superhydrophobic surface. (a) Two fracture modes and the corresponding internal crack propagation directions. δ represents the vertical direction, and τ represents the horizontal direction. (b) Adhesion strength curve of the surface ice layer. The red straight line indicates the phase where ice adhesion strength increases and decreases, the blue straight line indicates the phase where ice adhesion strength stabilizes, and the red wavy line indicates the phase where the minimum ice adhesion is reached. (c) Ice block fracture mode on the surface. The arrows indicate the direction of the de-icing force, the red dashed line represents the initial position of the ice block, and Lc is the length of the compressed region of the ice block. (d) Ice adhesion strength on superhydrophobic surface under three different environmental pressures. The inset shows the testing process and infrared images. (e) and (f) Show the ice layer and interface contact types under 95 kPa and 60 kPa pressures, respectively. The curves represent the evaporation process, with the blue arrows indicating the steam reaction force and the red arrows representing the ice layer detachment direction [49]. Copyright © 2025 Elsevier Masson SAS. All rights are reserved, including those for text and data mining, AI training, and similar technologies.

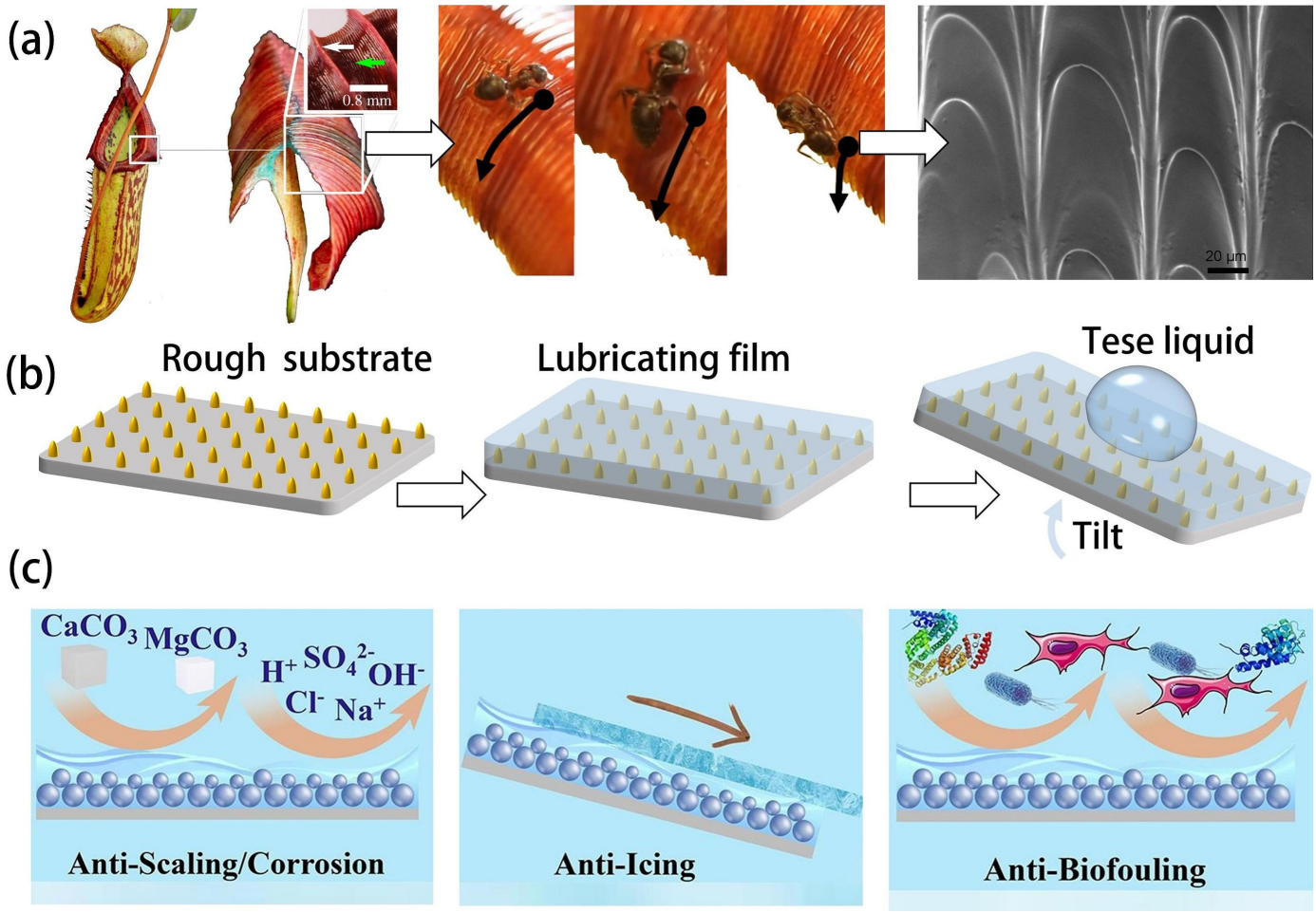


Figure 5. Design principles and applications of pitcher plant. (a) the structure of pitcher plant peristome and the locomotion behavior of ants on the peristome. (b) forms a physically smooth and chemically uniform lubricating film on the substrate surface. (c) the application of SLIPS function surface in different fields [55]. Copyright © 2024 Elsevier B.V. All rights reserved.

significantly reduced, typically by one or two orders of magnitude compared to conventional surface.

Stress concentration effect. When a small external force, such as wind, vibration, or gravity, is applied to the ice layer, the ice is anchored only at a few structural tips. This leads to a high concentration of stress at these narrow contact points. These localized stress concentrations often exceed the fracture strength of the contact points, causing brittle failure of the ice layer at its root. Consequently, the entire ice layer may easily fracture or flake off the surface.

Interface defects and crack propagation. Numerous natural defects and voids exist at the ice-solid interface and within the air-filled cavities of the micro-nanostructures. When the ice layer is subjected to heat or external forces, cracks tend to nucleate and rapidly propagate at these defects, thereby weakening the ice-solid bond and accelerating the overall detachment of the ice layer.

In fact, the above-mentioned de-icing or anti-icing mechanisms on superhydrophobic surface do not exist in isolation. They often work synergistically. For example, delaying the onset of ice formation creates a time window for external forces (such as wind or airflow during aircraft takeoff) to remove the water droplets before they freeze. Even if freezing occurs, the low ice adhesion strength requires very little energy for de-icing. Moreover, SHS can also be combined with other technologies to form new composite anti-icing materials.

2.4 Slippery Liquid-infused Porous Surface Technology

To overcome the shortcomings of superhydrophobic surface, in 2011, Aizenberg and colleagues developed the SLIPS technology inspired by the structure of the Nepenthes [50]. The peristome of Nepenthes is coated with a slippery lubricant, causing insects to lose footing and slide into the pitcher upon contact [51].

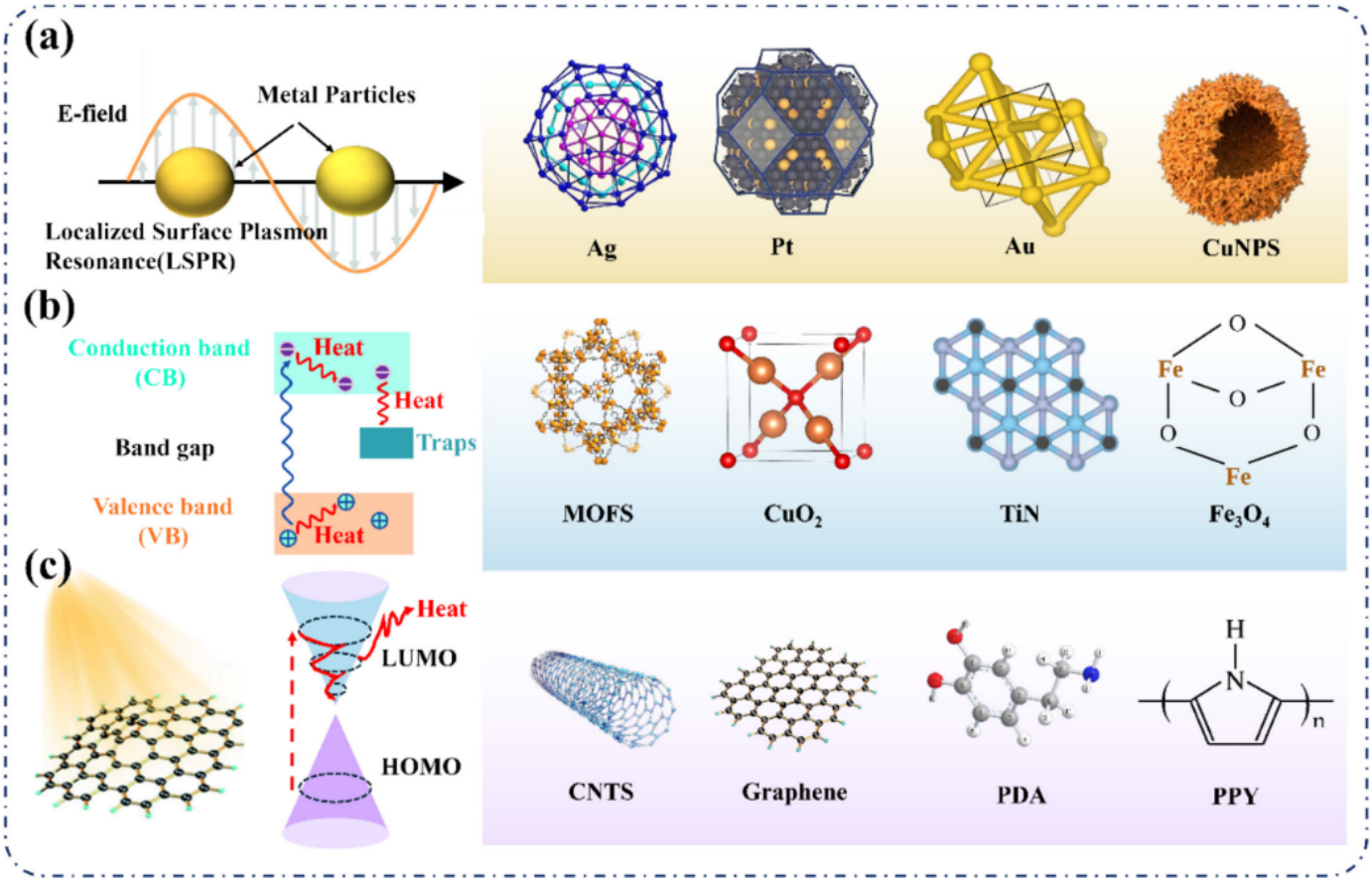


Figure 6. Three fundamental mechanisms in photothermal conversion materials. (a) Localized surface plasmon resonance and related materials. (b) Non-radiative relaxation and related materials (c) Molecular thermal vibration and related materials [57]. Copyright @ 2013 Royal Society of Chemistry.

Furthermore, its internal surface features a two-level hierarchical architecture of radial ridges [52], which enables vertical, gradient-driven directional water transport (Figure 5). Moreover, there are three design criteria for SLIPS: (1) the lubricant must have the ability to penetrate, wet, and securely adhere to the substrate; (2) the substrate should exhibit a preference for being wetted by the lubricant over external liquids, thereby avoiding displacement; (3) the lubricant and external liquids must be immiscible [50]. In order to satisfy these criterions, a thorough understanding of the physical and chemical properties of both the lubricant and substrate is necessary. Therefore, by combining a superhydrophobic surface with a lubricating liquid, a lubricating liquid film is formed. This film provides lubrication, making it difficult for the ice layer to adhere to the surface. Even if frost forms, it will bond with the lubricating film rather than the solid surface, further reducing the ice's adhesion. When the external temperature rises or physical vibrations occur, the ice layers easily detach. The mechanisms behind this include:

Low friction and low adhesion. The presence of the lubricating layer significantly reduces both friction and adhesion on the surface. Even at low temperatures, the friction and adhesion between the ice and the superhydrophobic surface are much lower than that of ordinary surface. As a result, ice crystals are less likely to stay or grow on the surface for extended periods, greatly enhancing the material's anti-icing properties.

Thermal transfer effect. In SLIPS materials, the lubricant layer acts as a thermal barrier, increasing heat transfer resistance and delaying ice nucleation. Therefore, optimizing the surface morphology and properties of the lubricant film can either enhance heat transfer rates or reduce the stability of surface ice crystals, thereby minimizing ice accumulation [53, 54]. Furthermore, the thermal properties of these materials are closely related to their freezing behavior, further boosting their anti-icing performance.

2.5 Photothermal Effect

Photothermal Effect refers to the phenomenon where materials convert absorbed light energy into heat energy. The solar radiation spectrum spans wavelengths from 150 to 4000 nm. The portion below

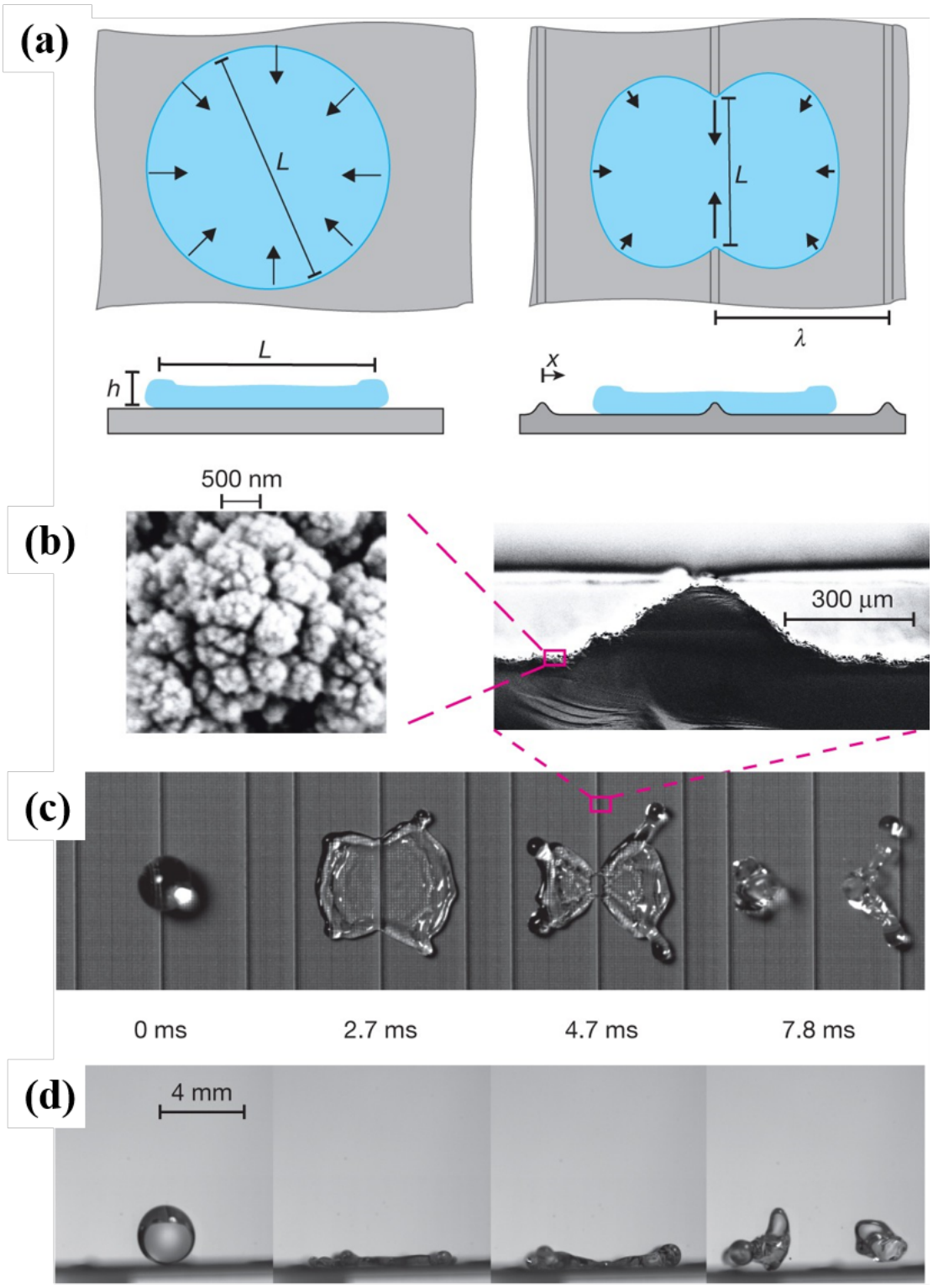


Figure 7. The correspondence between structural design and droplet motion. (a) The retraction speed of a film increases with decreasing thickness. Left and right, diagrams of a macroscopically untextured surface and a macroscale textured surface, respectively; top and bottom, top-view and side-view diagrams illustrating how macroscale texturing can modify the thickness profile of the drop, leading to variations in recoil speed (indicated by the length of the arrows). (b) As shown in these SEM images, we have fabricated a silicon surface with both submicrometre roughness and structure on a macroscopic (-100 μm) scale by laser ablation. (c) When a drop impacts the surface with the macroscopic structure, it moves rapidly along the ridge as it recoils. (d) Simultaneous high-speed images captured from the side reveal that the overall contact time is reduced by 37% to 7.8 ms [64]. Copyright © 2013, Springer Nature Limited.

Table 1. Comparison of characteristics of three superhydrophobic surfaces.

Coating type	Typical performance indicators	Advantages	Disadvantage	Key influencing factors of cost	Application scenarios	Ice Adhesion Strength (Typical Range)	Ice Delay Time (@ -10°C)
Conventional Anti-Icing Superhydrophobic Surfaces	Solid-liquid contact time	Significantly inhibits the impact icing of supercooled droplets	The anti-icing effect is significantly diminished under high humidity and low temperature conditions	Array precision	Non-extremely low temperature scenarios with low environmental humidity	100 - 400 kPa [102, 103]	5- 15 min
Slippery liquid-infused porous and superhydrophobic surfaces	Solid-liquid contact time	Smooth surface, with extremely low ice adhesion; Effectively cope with high humidity environments	The lubricating layer is at risk of depletion and requires regular maintenance	Types of lubricating agent	Scenarios where the requirement for ice adhesion is extremely low and condensation may occur	20 - 150 kPa [104]	10 - 35 min
Photothermal superhydrophobic surface	Photothermal de-icing time	Strong active ice-melting capability, can quickly remove the formed thin ice and prevent ice accumulation.	When there is insufficient light, the photothermal efficiency drops sharply, and the anti-icing capability fails.	Types of photothermal materials	Anti-icing scenarios with stable illumination	10 - 100 kPa [105]	10 - 40 min

400 nm falls within the UV range, contributing about 5% of the total energy. The visible spectrum (400 – 760 nm) accounts for approximately 46% of the total energy, while the near-infrared (NIR) region (760–2500 nm) contributes about 49% [37]. Thus, effective photothermal conversion materials should have strong light absorption within the 250–2500 nm range and high photothermal conversion efficiency. Photothermal conversion mechanisms can be primarily grouped into three main categories: localized surface plasmon resonance (LSPR) (Figure 6 (a)), non-radiative relaxation (Figure 6 (b)), and molecular thermal vibration (Figure 6 (c)). The specific mechanism is as follows: Photothermal materials, such as metallic nanoparticles and carbon-based materials, interact with photons at specific wavelengths, causing electrons within the material to transition from their ground state collisions and thermalization, exchange energy with surrounding atoms and molecules, intensifying the vibration then transferred to the contact surface, achieving thermal diffusion and a heat transfer gradient [56]. Moreover, when combined with superhydrophobic materials, this effect can further enhance the anti-icing performance of SHS. The de-icing effect of photothermal action is as follows:

Raising Surface Temperature. The photothermal effect rapidly heats the surface, increasing its temperature, preventing the formation of ice crystals or causing already attached ice and snow to melt. Under illuminated conditions, these materials efficiently convert light energy into heat, raising the surface temperature above the melting point of ice, thus achieving de-icing.

Preventing Ice Adhesion. The heating effect of photothermal materials helps maintain the surface temperature above the critical anti-icing threshold, effectively preventing the adhesion of frost or snow. When the surface material is hydrophobic or superhydrophobic, localized heating further reduces the adhesive force of ice crystals, thereby accelerating the removal of ice and snow.

3 Design and preparation of Multifunctional Anti-Icing Superhydrophobic Surface

Traditional superhydrophobic surface achieves a reduction in the solid–liquid contact area primarily through the construction of micro-/nano-scale roughness and the incorporation of low surface energy materials, thereby theoretically mitigating ice formation [58]. However, such surfaces are generally static in nature—their anti-icing performance is inherently passive and lacks the ability to dynamically respond to external stimuli [59]. Consequently, their adaptability to varying environmental conditions is limited. To address these shortcomings, the objective is to introduce additional functional mechanisms or to optimize surface microstructures in order to enhance multifunctionality, environmental adaptability, and long-term durability. Three typical anti-icing superhydrophobic designs are shown in Table 1, these advancements offer more effective and robust solutions for anti-icing applications.

3.1 Conventional Anti-Icing Superhydrophobic Surface

By designing the protrusion structures and surface roughness of SHS, the interaction between droplets and the substrate—as well as droplet mobility—can

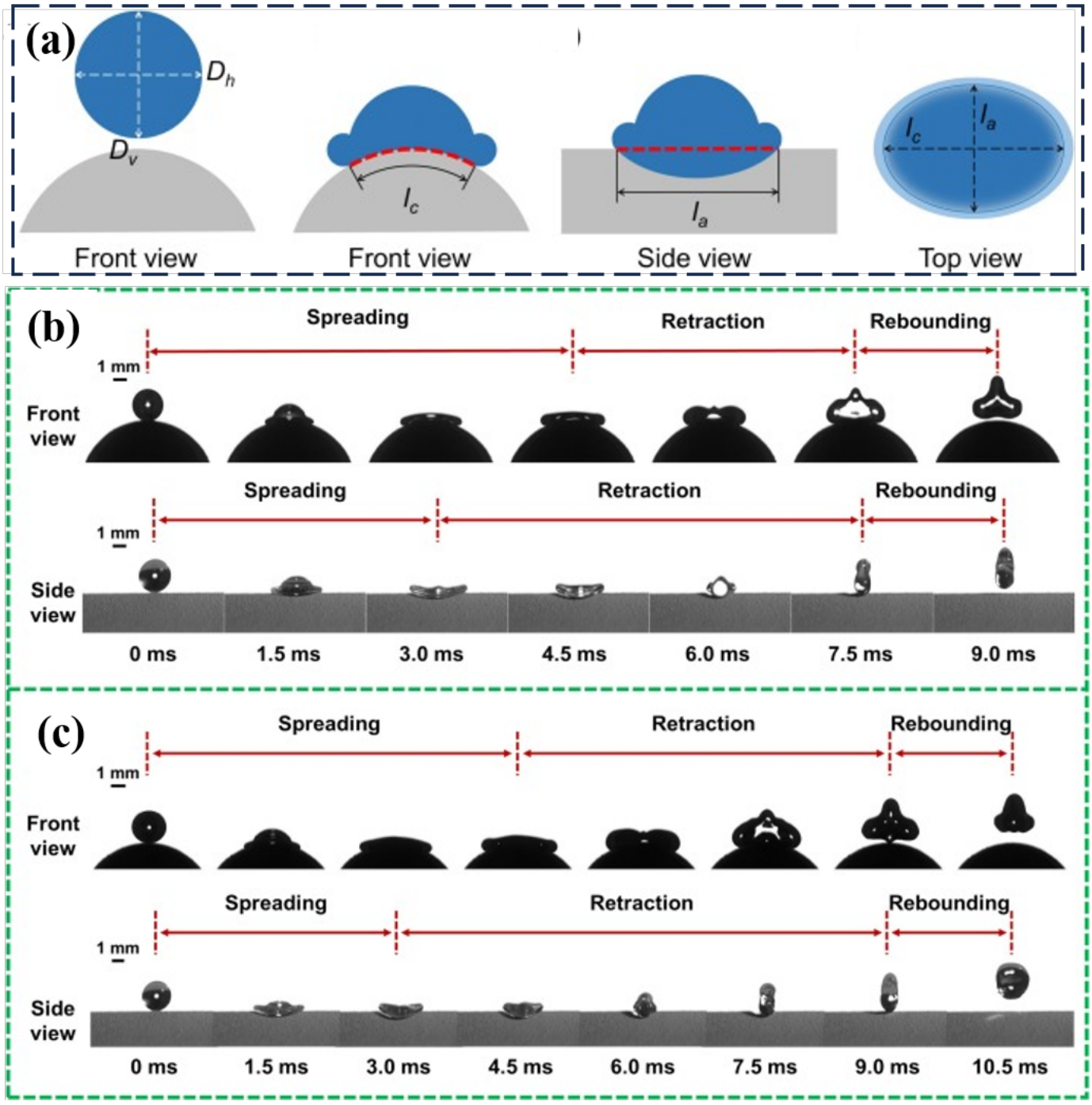


Figure 8. Droplet impact process on a SHS. (a) Schematic diagram of the parameters during the droplet impact process on cylindrical surfaces. Upon impact, droplets spread both axially and circumferentially along the cylindrical surface. The circumferential spreading factor is defined as $\beta_c = l_c/D_0$, where l_c is the circumferential spreading length. Similarly, the axial spreading factor is defined as $\beta_a = l_a/D_0$, where l_a is the axial spreading length. D is the diameter of the cylindrical surface. (b) Sequential images of droplet impact, $D = 9$ mm, $H = 3$ cm, $T_s = 25°C$. (c) Sequential images of droplet impact process, $D = 9$ mm, $H = 4$ cm, $T_s = -15°C$. The time taken for droplets to spread in the circumferential direction was longer than in the axial direction. The axial contraction initiated even as the droplet continued to spread along the circumferential direction. The axial retraction fluid would pull back the fluid still spreading in the circumferential direction, leading to earlier rebounding compared to planar surfaces, despite a longer circumferential spreading time [65]. Copyright © 2025 Elsevier Inc.

be precisely regulated, thereby enhancing anti-icing performance. From the perspective of ice nucleation, the freezing of stationary liquid droplets is generally initiated either by microscopic impurities within the droplet (heterogeneous nucleation) or by the spontaneous arrangement of water molecules

at sufficiently low temperatures (homogeneous nucleation) [60]. Nucleation typically occurs under low degrees of supercooling and proceeds at a relatively slow rate [61].

However, when a supercooled droplet impacts a surface at high velocity, it experiences a substantial transient pressure. This sudden pressure compresses the molecular structure of the droplet, increasing the local liquid density. According to classical nucleation theory, an increase in system pressure elevates the chemical potential of the liquid phase, thereby reducing the critical free energy barrier for nucleus formation and facilitating nucleation [62]. Furthermore, the droplet undergoes rapid deformation upon impact, substantially increasing its SHS. On conventional smooth surfaces, axisymmetric receding occurs, where the droplet edge retracts uniformly inward while the center remains largely stationary. The receding speed in such cases is governed by the thickness of the liquid film (Figure 7(a)). In contrast, the introduction of periodic ridges results in non-axisymmetric, center-assisted receding. This design causes variations in the film thickness across the droplet, with thinner regions—requiring less mass to accelerate—receding more quickly. Simultaneously, the structured texture facilitates the involvement of the droplet center in the retraction process, thereby reducing both the overall retraction distance and the contact time (Figure 7(b)). Specifically, the contact time decreased from 12.4 ms on a smooth surface (Figure 7(d)) to just 7.8 ms on the patterned surface (Figure 7(c)), representing a 37% reduction. Shorter contact times limit the heat transfer between the droplet and the cold substrate, thereby suppressing phase transition. Even if ice nuclei are generated, the insufficient thermodynamic driving force prevents their further growth [63].

During the rebound process of a droplet, the curvature of the surface structure affects the rebound shape and contact time of the droplet. The results of Guo et al. [65] show that as the curvature diameter increases, the rebounding droplet gradually becomes more intact from its initial rupture (Figure 8). Meanwhile, arrays composed of ordered microstructures—such as pillar or conical elements—can further guide droplet spreading and retraction dynamics. Upon impact, the mass redistribution and central retraction of the droplet promote rapid rebound, resulting in the so-called "pancake bounce" phenomenon [46]. This unique bouncing behavior involves the droplet briefly adopting a flattened morphology before re-forming into a sphere, significantly reducing its contact time with the surface—by as much as 60% to 80% [66]. By carefully tuning the dimensional parameters of these arrays, it is possible to increase the critical humidity and volume thresholds required for a condensation-induced transition from the Cassie–Baxter state to the Wenzel state. This effectively suppresses condensation within the structured array, helping to preserve the Cassie–Baxter state and maintain the superhydrophobic performance.

Despite their potential, realizing SHS arrays capable of exhibiting the pancake bounce effect requires structures with diameters below 100 μm and aspect ratios greater than 10. Large-scale fabrication of such high-aspect-ratio microstructures remains technically challenging [67]. As the surface area increases, manufacturing costs rise, and issues such as process inconsistency and structural defects may arise, ultimately affecting product reliability [68]. Moreover, the pancake bouncing effect depends on highly specific conditions, such as precise surface temperature and humidity levels. This necessitates exact control over both droplet impact parameters and surface morphology, as the phenomenon is highly sensitive to ambient humidity and external disturbances [69]. And fabricating the required hierarchical micro-nano structures typically involves precision etching techniques. Overcoming these material and control challenges will be key to enabling the large-scale, practical deployment of durable superhydrophobic surfaces in real-world anti-icing applications.

3.2 Slippery Liquid-infused Porous and Superhydrophobic Surface

Slippery Liquid-Infused Porous Surface (SLIPS) exhibit a high degree of hydrophobicity, characterized by a contact angle hysteresis of less than 2.5° and a rolling angle of less than 5° [53]. These materials consist of two phases: a solid substrate and a surface lubricant. In comparison to superhydrophobic surface, SLIPS demonstrate relatively smooth and stable characteristics. The design of the substrate plays a crucial role in determining the overall performance of SLIPS, particularly in enhancing wettability and maintaining lubricant retention [70]. Through capillary action [71], van der Waals forces [72], hydrogen bonding [73], and other interactions, liquids are securely anchored within the rough microstructures of the substrate. Compared to solid surface, SLIPS offer superior adaptability in extreme

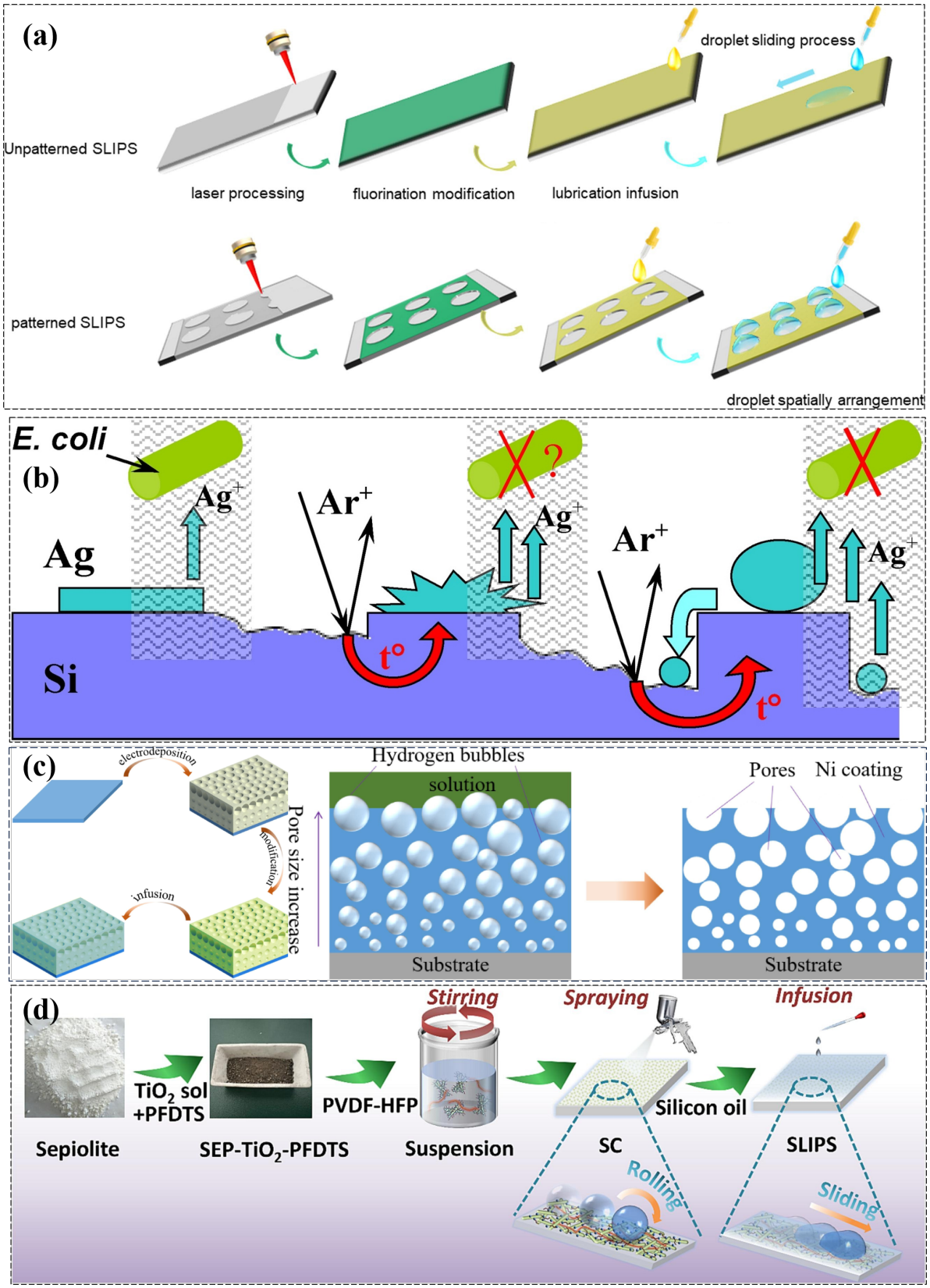


Figure 9. SLIPS preparation technology. (a) Laser scanning on PET surface to fabricate unpatterned and patterned SLIPS [76]. Copyright © 2024 Elsevier B.V. All rights reserved. (b) Photolithography methods [77]. (c) The construction process of slippery surface by templating [78]. Copyright © 2020 Elsevier B.V. All rights reserved. (d) Schematic demonstration of SLIPS preparation and liquid repelling characteristics by incorporating nanoparticles [79]. Copyright © 2024 Elsevier B.V. All rights reserved.

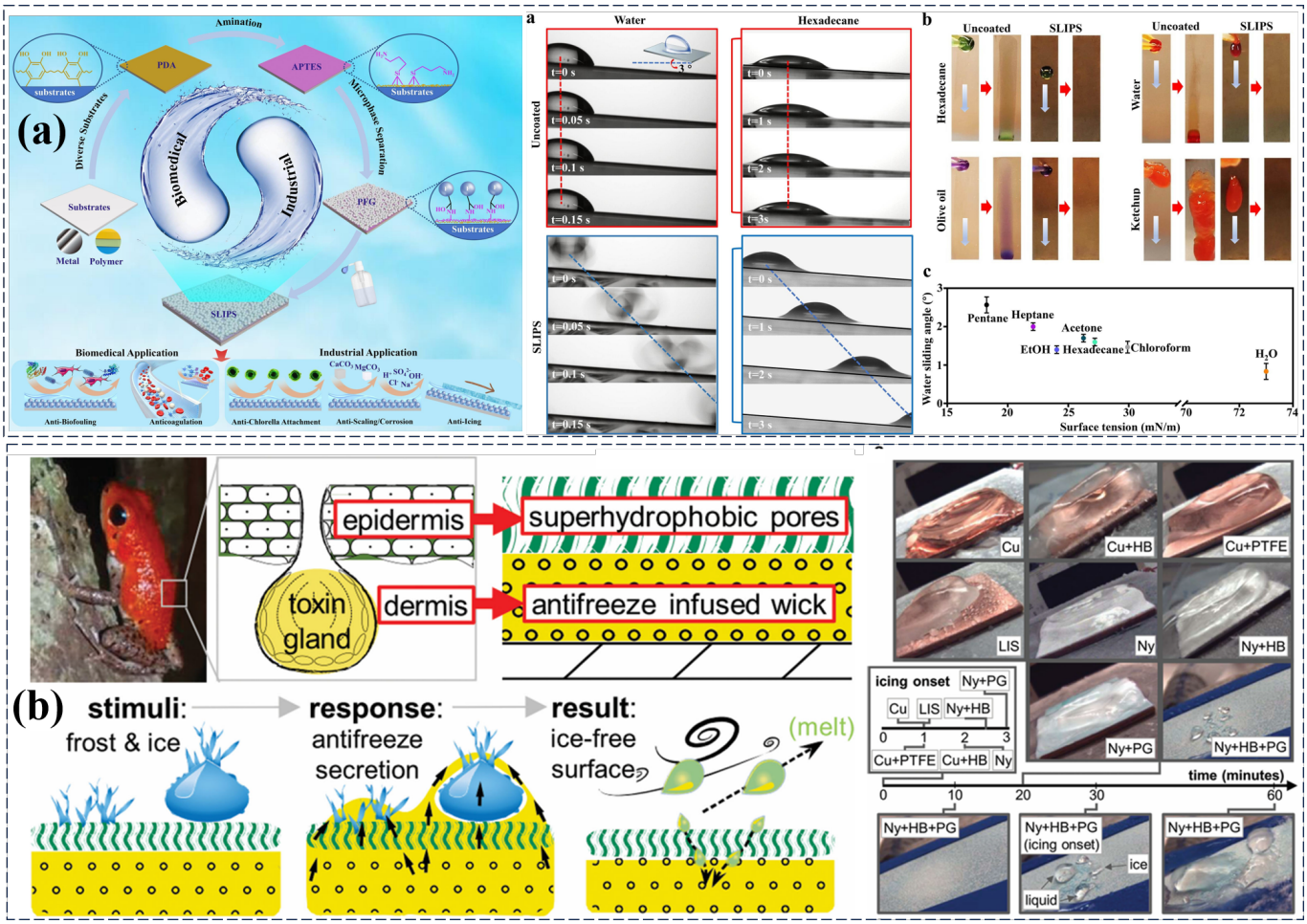


Figure 10. Several slippery liquid-infused and superhydrophobic surface. (a) modification strategy, slippery performance and liquid-repellency behavior of the SLIPS. SLIPS coating was facilely constructed on various substrates and shapes in bulk through a facile and effective step-by-step deposition strategy. In particular, the spontaneous microphase separation on the surface induced by the prominent polar differences between the superhydrophobic fluorinated segments and hydrophilic hydroxyl and amino groups enabled ultra-stable perfluocarbon oil loading, ensuring superior anti-fouling, anti-corrosion, anti-icing and anti-scaling performances with high robustness [84]. copyright© 2024 Elsevier Inc. All rights are reserved, including those for text and data mining, AI training, and similar technologies. (b) schematic of the stimuli-responsive antifreeze secreting anti-icing coating inspired by the functionality and bilayer architecture of a poison dart frog skin. The porous superhydrophobic epidermis separates the antifreeze infused dermis from the environment. And the antifreeze liquid is secreted through the pores in response to contact with ice or frost forming on the surface, which results in melting of the ice or frost. Subsequently, the melt is removed via air motion or partially wicked back into the dermis [86]. Copyright © 2015 WILEY-VCH Verlag GmbH & Co. KGaA, Weinheim.

environments characterized by high pressure and humidity, and they are capable of withstanding external impacts and friction. Additionally, SLIPS possess self-cleaning and self-healing properties, allowing them to recover their original state following damage or contamination [74].

The most common Slippery Liquid-Infused Porous Surface (SLIPS) utilize various low-surface-energy organic liquids for lubrication. These materials are straightforward to prepare and exhibit excellent surface stability. The preparation of SLIPS typically follows a two-step process, involving substrate fabrication and lubricant infusion. Substrate preparation methods can be categorized into two approaches: top-down and bottom-up techniques. Methods such as chemical etching, laser etching [75, 76], photolithography [77], templating [78], or the incorporation of micron/nanoparticles into coatings to construct micro- and nano-structures [79] are employed to create the rough surface, followed by the infusion of lubricating oils to form the slippery surface (Figure 9).

Perfluoropolyether (PFPE) [80], known for its ultra-low surface energy and high stability, serves as an effective lubricant for SLIPS. A simple processing

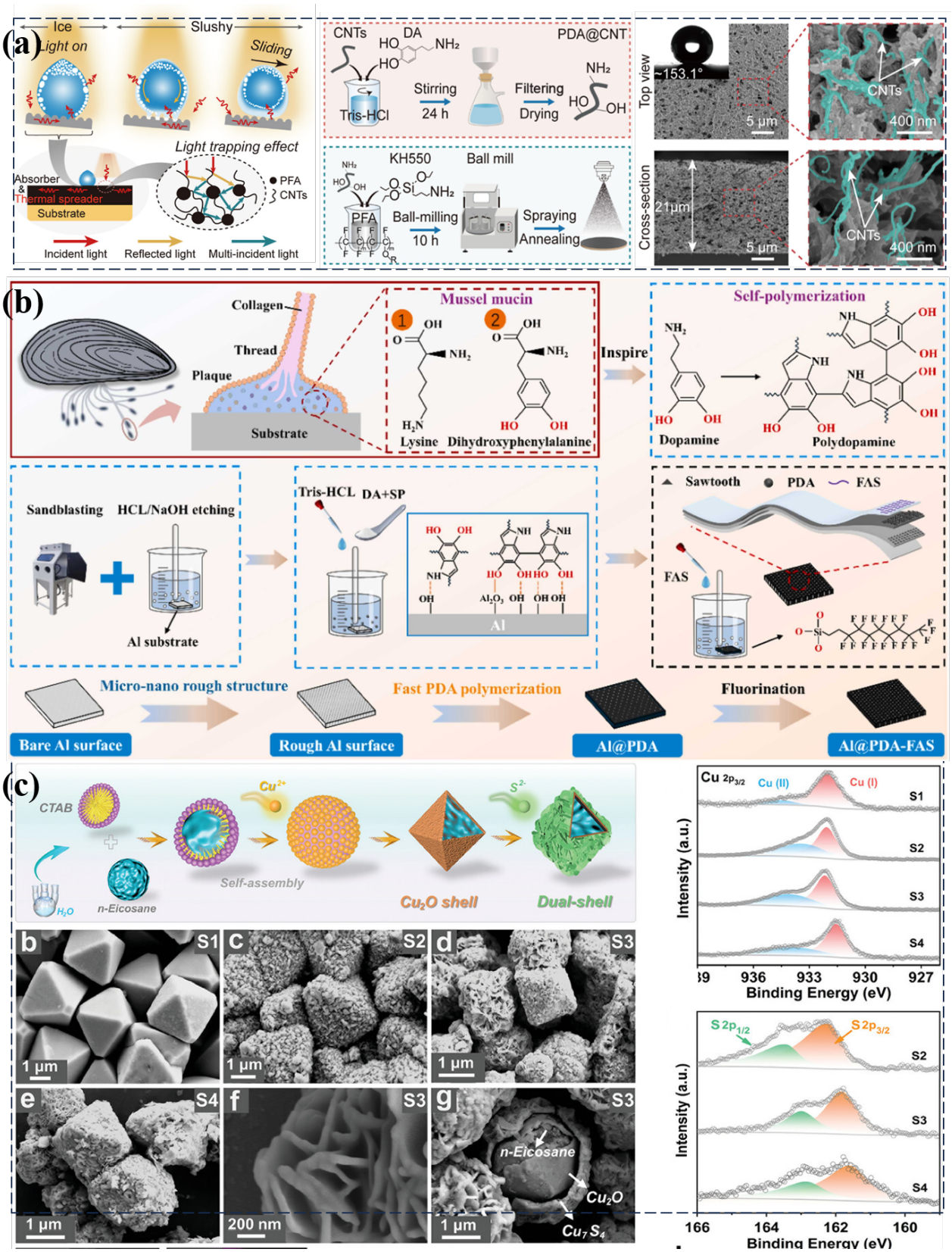


Figure 11. Several photothermal superhydrophobic surface. (a) Fabrication and characterization of the PFA-CNT coating [94]. Copyright © 2025 American Chemical Society. (b) Fabrication process of photothermal superhydrophobic coatings based on fast polymerization of PDA on Al substrates inspired by mussel wet adhesion ability [95]. Copyright© 2025 Elsevier B.V. All rights are reserved, including those for text and data mining, AI training, and similar technologies. (c) Preparation and characterization of the dual-shell microcapsules [96]. Copyright © 2023 Wiley-VCH GmbH.

method has been developed by injecting PFPE into porous polyvinylidene fluoride-hexafluoropropylene copolymer (PVDF-HFP) membranes, which are prepared through non-solvent induced phase separation (NIPS), achieving processing times of less than five minutes. PFPE-infused SLIPS demonstrate exceptional stability in industrial applications, including anti-icing, corrosion resistance, anti-fouling, as well as anti-adhesion and antimicrobial properties for medical and biomedical applications [81]. However, the environmental risks associated with perfluoralkyl substances, due to potential contamination, limit the widespread use of PFPE. Consequently, alternative lubricants, such as silicone oils, lipids, and solid lubricants like graphite and MoS_2 [82], are being explored.

Inspired by the structures of the Nepenthes pitcher plant and slicing paraffin [83], Yang et al. [84] developed a Multifunctional aluminum alloy slippery liquid-infused surface by infused paraffin and silicone oil into superhydrophobic aluminum (Figure 10(a)). This materials delays icing by 560 s at -15 ℃ and 231 s at -30 ℃, offering remarkable anti-icing and deicing performance. Polydimethylsiloxane (PDMS), a polymer known for its excellent chemical and physical stability, is considered an ideal hydrophobic agent due to its non-toxic, odorless nature and its ability to operate across a wide temperature range (-50 ℃ to 200 ℃). Golovin et al. [85] utilized Sylgard 184 (a PDMS precursor) to lubricate polymer-based elastomeric de-icing surface, comparing strength-limited deicing with toughness-limited deicing. the results show that for PDMS-lubricated samples, ice adhesion averaged only 14–16 kPa, significantly lower than the ordinary samples.

Additionally, ethylene glycol, known for its hygroscopic nature, is commonly used in organic antifreeze agents. Sun et al. [86] developed an anti-icing material with a superhydrophobic epidermis and a porous dermis structure inspired by the functionality and bilayer architecture of a poison dart frog skin. It slows condensation on this heterogeneous surface and antifreeze diffusion into drops slowed icing-onset and complete icing-over of the surface by a remarkable 1000% and 2000% as compared to the control samples (i.e., 30 and 60 min vs <3 min) (Figure 10(b)). Under extreme low-temperature conditions, the surface was found to release the antifreeze, forming a lubricating layer that facilitated ice removal. These results demonstrate that the prepared material requires antifreeze replenishment to restore the anti-icing performance of the coating. While Slippery Liquid-Infused Porous (SLIP) surfaces demonstrate remarkable low-adhesion and self-cleaning capabilities, their practical deployment is hindered by critical limitations. The infused lubricant layer is susceptible to gradual depletion through evaporation, wearing, or displacement by contaminants, resulting in progressive performance loss. Additionally, the functionality of many lubricants is compromised at low temperatures due to excessive viscosity increase, freezing, or phase separation. To overcome these challenges, future efforts should focus on the design of novel lubricants with minimal temperature-dependent viscosity and enhanced freeze-thaw stability. In parallel, engineering structures capable of storing and controllably replenishing lubricant could substantially improve the durability and long-term reliability of SLIP surfaces, enabling their robust and sustained real-world application.

3.3 Photothermal Superhydrophobic Surface

In low-temperature and high-humidity environments, superhydrophobic surface can still freeze and form an interlocking structure with the ice, which increases the adhesion strength of the ice [87]. To mitigate photothermal materials. These materials convert light energy into thermal energy using solar or other light sources to actively heat the surface, reducing ice adhesion or directly melting the ice layer [88]. The photothermal materials must have high solar absorptivity while preserving the original properties of the coating. Based on the type of material, these can be categorized into carbon-based photothermal conversion materials, such as graphene [89] and carbon nanotubes [90], as well as metal nanoparticles, including Fe_3O_4 [91], TiO_2 [92], and TiN [93], along with other semiconductor materials.

A significant challenge in utilizing photothermal materials is their mechanical instability, which may cause particle detachment and performance degradation. To overcome this, matrix materials with excellent mechanical properties are used alongside robust photothermal materials. For example, Li et al. [94] employed perfluoroalkoxy (PFA) polymer as the matrix due to its exceptional mechanical strength and toughness, offering resistance to physical wear and deformation. Carbon nanotubes (CNTs), known for their high aspect ratio and superior mechanical properties, were selected as the photothermal agent. Uniformly dispersed in the PFA matrix, CNTs form a

skeletal support structure that enhances the coating's tensile and impact resistance. A silane coupling agent (KH550) was used to improve the interfacial compatibility between CNTs and PFA, reducing interfacial defects and preventing delamination under stress. Extensive experimental results confirmed its superior mechanical, chemical, and thermal durability (Figure 11(a)). The coating achieved a solar absorptance of 97.7% and improved thermal conductivity by 280% compared to pure polymer matrices. Even under weak light and extremely low temperatures, the coating demonstrated excellent de-icing performance on actual power lines and residential rooftops.

However, most mainstream photothermal materials are inherently opaque, which limits their use in applications requiring optical transparency, such as sensor and detector surface. To address this, Li et al. [97] developed a transparent photothermal coating by combining polyacrylic acid with near-infrared (NIR)-absorbing cesium tungsten bronze nanoparticles and ultraviolet (UV)-absorbing methylene bis-benzotriazolyl tetramethylbutylphenol. The resulting coating exhibits high transmittance in the visible spectrum while strongly absorbing UV and NIR light. This synergistic design allows water droplets on the surface to remain unfrozen for at least one hour without sunlight and resist icing for extended periods under illumination, with stable anti-icing performance down to –25°C and even as low as –30°C in extreme conditions. Wu et al. [95] developed a robust photothermal superhydrophobic coating with excellent mechanochemical and icing-melting durability, based on mussel-inspired adhesion chemistry (Figure 11(b)). The icing delay time was significantly extended to 436 s, and the photothermal ice-melting time was shortened to 65 s, demonstrating both anti-icing and de-icing performance.

Although emerging photothermal anti-icing materials can achieve rapid de-icing through efficient light harvesting, their continuous photothermal effect may lead to surface overheating during hot summer conditions, which accelerates material aging and increases the risk of thermal failure. To resolve this issue, Yao et al. [98] proposed a dynamic wettability-switching strategy. Using an eco-friendly, fluorine-free spray-coating method, they developed an intelligent coating (PSTM) by combining dual-scale hydrophobic TiO_2 nanoparticles (for hierarchical roughness) with a photothermal network of multi-walled carbon nanotubes (MWCNTs). Performance tests showed that PSTM delayed icing by 2248 s at -10°C and achieved complete de-icing within 283s under 1 sun illumination (1000 W/m^2). Moreover, photothermal superhydrophobic surface exhibits passive anti-icing performance, which diminishes under low-light conditions, such as nighttime, cloudy days, or shaded areas, where no energy input is available to prevent icing. In such scenarios, photothermal heating is activated. Additionally, in low-light or emergency situations, the system switches to electric heating to provide supplemental energy, ensuring all-weather active de-icing [99]. For example, a multilayer functional film that combines CNT-based electric heating layers with cobalt-based photothermal properties and SiO_2 for roughness and light trapping has been demonstrated to reduce energy consumption while enhancing de-icing efficiency [100]. Phase change materials (PCMs) also present a promising solution to the intermittency of solar energy (Figure 9(c)). PCMs store solar energy during the day as latent heat and release it gradually during the night or in low-light conditions, maintaining surface temperature and delaying icing or aiding in de-icing [96, 101]. Although photothermal superhydrophobic surface exhibits considerable promise for active anti-icing applications, their practical deployment is constrained by several key challenges. A major limitation is their strong reliance on external light sources, which restricts performance under low-illumination or nighttime conditions. Furthermore, the intricate micro-nano structures essential for superhydrophobicity are often vulnerable to mechanical abrasion and environmental contamination, compromising long-term durability. Achieving an optimal balance between high photothermal conversion efficiency and stable hydrophobic properties remains materially and structurally challenging. These issues, compounded by difficulties in achieving scalable and uniform manufacturing, have hindered widespread adoption. Overcoming these barriers will require interdisciplinary advances in material design, surface engineering, and processing techniques.

4 Conclusions and Perspectives

This review, grounded in the fundamental principles of interfacial wettability, systematically elucidates the mechanisms underlying the anti-icing and de-icing performance of SHS. Extensive research has demonstrated that the superior ice-phobic behavior of SHS primarily stems from a markedly delayed freezing onset and a substantial reduction in ice

adhesion strength. These effects arise from the transition of liquid–solid interaction from surface contact to point contact, coupled with the enhanced self-propelled jumping of condensate droplets that suppresses ice nucleation and bridge formation. Building on these passive mechanisms, recent studies have explored synergistic strategies—such as integrating super-lubricity, photothermal conversion, and other active functionalities—to further improve de-icing efficacy and broaden the application scope of SHS. Despite these advances, durability remains a central challenge that limits the reliability of SHS under complex and harsh environments. Current coatings are prone to significant performance degradation when exposed to high humidity, salt spray, ultraviolet radiation, mechanical abrasion, and repeated freeze–thaw cycling. Environmentally sustainable and long-lifespan SHS materials remain at an early developmental stage. Moreover, the lack of standardized test protocols and industrial benchmarks hampers the engineering translation of SHS, preventing their widespread adoption in sectors with stringent operational demands, such as aerospace and energy infrastructure.

To accelerate the practical deployment of robust and scalable SHS for de-icing applications, future research should focus on the following directions:

(1) Development of next-generation SHS materials. Designing multifunctional composite coatings that integrate superhydrophobicity with photothermal or electrothermal conversion, phase-change components, or adaptive surface chemistries to enable long-term stability under extreme environmental conditions.

(2) Multiscale modeling and simulation of icing phenomena. Establishing comprehensive coupled physicochemical models that capture the full icing cycle—from nucleation and crystal growth to interfacial adhesion and detachment—supported by integrated computational and experimental validation to guide rational structural design and performance optimization.

(3) Green, scalable, and cost-efficient fabrication strategies. Developing sustainable raw materials and environmentally benign manufacturing routes that reduce processing complexity and costs, thereby facilitating large-scale industrial implementation without compromising functionality.

(4) Standardized evaluation and engineering qualification. Formulating unified testing frameworks that assess key indicators such as abrasion resistance, weatherability, long-term durability, and freeze–thaw stability. Close alignment with industrial standards will be essential to bridge laboratory research with engineering deployment and commercialization.

Overall, the convergence of mechanism-driven design, multifunctional integration, sustainable fabrication, and standardized engineering evaluation will be critical for enabling the next generation of SHS capable of delivering reliable, durable, and energy-efficient de-icing and anti-icing performance in real-world environments.

Data Availability Statement

Not applicable.

Funding

This work was supported by the Open Project of National Key Laboratory for Materials in Major Infrastructure Engineering under Grant EMMI2025210.

Conflicts of Interest

The authors declare no conflicts of interest.

AI Use Statement

The authors declare that no generative AI was used in the preparation of this manuscript.

Ethical Approval and Consent to Participate

Not applicable.

References

[1] Barthlott, W., & Neinhuis, C. (1997). Purity of the sacred lotus, or escape from contamination in biological surfaces. *Planta, 202*(1), 1–8. [CrossRef]

[2] NEINHUIS, C., & BARTHLOTT, W. (1997). Characterization and Distribution of Water-repellent, Self-cleaning Plant Surfaces. *Annals of Botany, 79*(6), 667–677. [CrossRef]

[3] Feng, L., Li, S. H., Li, Y. S., Li, H. J., Zhang, L. J., Zhai, J., Song, Y. L., Liu, B. Q., Jiang, L., & Zhu, D. B. (2002). Super-hydrophobic surfaces: From natural to artificial. *Advanced Materials, 14*(24), 1857–1860. [CrossRef]

[4] Feng, L., Zhang, Z. Y., Mai, Z. H., Ma, Y. M., Liu, B. Q., Jiang, L., & Zhu, D. B. (2004). A

super-hydrophobic and super-oleophilic coating mesh film for the separation of oil and water. *Angewandte Chemie-International Edition, 43*(15), 2012–2014. [CrossRef]

[5] Jiang, L., Zhao, Y., & Zhai, J. (2004). A lotus-leaf-like superhydrophobic surface: A porous microsphere/nanofiber composite film prepared by electrohydrodynamics. *Angewandte Chemie-International Edition, 43*(33), 4338–4341. [CrossRef]

[6] Young, T. (1805). III. An essay on the cohesion of fluids. *Philosophical transactions of the royal society of London*, (95), 65-87. [CrossRef]

[7] Zhao, J., Gao, X., Chen, S., Lin, H., Li, Z., & Lin, X. (2022). Hydrophobic or superhydrophobic modification of cement-based materials: A systematic review. *Composites Part B-Engineering, 243*, 110104. [CrossRef]

[8] Fabien, A., Lefebvre, G., Calvignac, B., Legout, P., Badens, E., & Crampon, C. (2022). Interfacial tension of ethanol, water, and their mixtures in high pressure carbon dioxide: Measurements and modeling. *Journal of Colloid and Interface Science, 613*, 847–856. [CrossRef]

[9] Wenzel, R. N. (1936). Resistance of solid surfaces to wetting by water. *Industrial & engineering chemistry, 28*(8), 988-994. [CrossRef]

[10] Wenzel, R. N. (1949). Surface Roughness and Contact Angle. *The Journal of Physical and Colloid Chemistry, 53*(9), 1466–1467. [CrossRef]

[11] Cassie, A. B. D., & Baxter, S. (1944). Wettability of porous surfaces. *Transactions of the Faraday Society, 40*(0), 546–551. [CrossRef]

[12] Luo, J., & Guo, Z. G. (2024). Recent advances in biomimetic superhydrophobic surfaces: focusing on abrasion resistance, self-healing and anti-icing. *Nanoscale, 16*(35), 16404–16419. [CrossRef]

[13] Nomeir, B., Lakhouil, S., Boukheir, S., Ait Ali, M., & Naamane, S. (2024). Durable and transparent superhydrophobic coating with temperature-controlled multi-scale roughness for self-cleaning and anti-icing applications. *Progress in Organic Coatings, 189*, 108338. [CrossRef]

[14] Wang, X., & Lin, Z. (2023). A novel high-performance coating with hybrid nanofiller reinforcement for superior self-cleaning, anti-icing, and corrosion resistance properties. *Journal of Building Engineering, 80*, 107993. [CrossRef]

[15] Zhang, B. B., Yang, G., Xu, W. C., Duan, J. Z., & Hou, B. R. (2024). Hybrid superamphiphobic anti-corrosion coating with integrated functionalities of liquid repellency, self-cleaning, and anti-icing. *Journal of Materials Science & Technology, 184*, 256–268. [CrossRef]

[16] Liu, S., Zhu, Z., Zheng, Q., Wang, K., Zhou, F., Yang, Q., Wang, X., Ye, L., Chen, Y., Liu, H., & Li, H. (2025). Waxberry-liked micro-nanostructured, superhydrophobic surfaces with enhanced photothermal de-icing and passive anti-icing properties. *Chemical Engineering Journal, 503*, 158358. [CrossRef]

[17] Lv, J., Song, Y., Jiang, L., & Wang, J. (2014). Bio-Inspired Strategies for Anti-Icing. *ACS Nano, 8*(4), 3152–3169. [CrossRef]

[18] Cao, L., Jones, A. K., Sikka, V. K., Wu, J., & Gao, D. (2009). Anti-Icing Superhydrophobic Coatings. *Langmuir, 25*(21), 12444–12448. [CrossRef]

[19] Xu, Z., Wang, G., Li, S., Li, D., Zhou, W., Yang, C., ... & Liu, Y. (2025). Thermodynamic mechanisms governing icing: Key insights for designing passive anti-icing surfaces. *iScience, 28*(2). [CrossRef]

[20] Lu, Y., Sathasivam, S., Song, J., Crick, C. R., Carmalt, C. J., & Parkin, I. P. (2015). Robust self-cleaning surfaces that function when exposed to either air or oil. *Science, 347*(6226), 1132-1135. [CrossRef]

[21] Zimmermann, J., Reifler, F. A., Fortunato, G., Gerhardt, L. C., & Seeger, S. (2008). A simple, one-step approach to durable and robust superhydrophobic textiles. *Advanced Functional Materials, 18*(22), 3662-3669. [CrossRef]

[22] Scarratt, L., Steiner, U., & Neto, C. (2017). A review on the mechanical and thermodynamic robustness of superhydrophobic surfaces. *Advances in Colloid and Interface Science, 246*, 133–152. [CrossRef]

[23] Wang, F., Liu, M., Liu, C., Zhao, Q., Wang, T., Wang, Z., & Du, X. (2022). Light-induced charged slippery surfaces. *Science advances, 8*(27), eabp9369. [CrossRef]

[24] Zhang, B. B., Xu, W. C., Xia, D. H., Fan, X. Q., Duan, J. Z., & Lu, Y. (2021). Comparison Study of Self-Cleaning, Anti-Icing, and Durable Corrosion Resistance of Superhydrophobic and Lubricant-Infused Ultraslippery Surfaces. *Langmuir, 37*(37), 11061–11071. [CrossRef]

[25] Anand, S., Paxson, A. T., Dhiman, R., Smith, J. D., & Varanasi, K. K. (2012). Enhanced Condensation on Lubricant-Impregnated Nanotextured Surfaces. *ACS Nano, 6*(11), 10122–10129. [CrossRef]

[26] Chen, F. Z., Wang, Y. Q., Tian, Y. L., Zhang, D. W., Song, J. L., Crick, C. R., Carmalt, C. J., Parkin, I. P., & Lu, Y. (2022). Robust and durable liquid-repellent surfaces. *Chemical Society Reviews, 51*(20), 8476–8583. [CrossRef]

[27] Gao, H., Yin, T., Ma, J., Zhou, Y., Li, K., & Bao, J. (2025). Research Progress of Photothermal Superhydrophobic Surfaces for Anti-Icing/Deicing. *Molecules, 30*(9), 1865. [CrossRef]

[28] Lin, Y., Chen, H., Wang, G., & Liu, A. (2018). Recent progress in preparation and anti-icing applications of superhydrophobic coatings. *Coatings, 8*(6), 208. [CrossRef]

[29] Nazari, A., & Eslami-Farsani, R. (2025). A review of photothermal and superhydrophobic polymer nanocomposites as anti-icing nanocoatings. *Polymer Composites, 46*(6), 5018-5040. [CrossRef]

[30] Niu, H., Yang, Y. I., & Parrinello, M. (2019). Temperature dependence of homogeneous nucleation in ice. *Physical review letters, 122*(24), 245501. [CrossRef]

[31] Chu, W., Nie, R., Chen, X., Wang, C., Gao, J., Wei, Z., ... & Guo, W. (2024). Heterogeneous Nucleation and Enhanced Charge Transfer via Amorphous Metal-Organic Frameworks for Efficient and Stable Perovskite Solar Cells. *Advanced Functional Materials, 34*(48), 2408829. [CrossRef]

[32] Guo, R., Cai, M., Zhao, J., Yang, P., Ying, H., & Zhang, K. (2024). Strategy for Regulation from Heterogeneous Nucleation to Homogeneous Nucleation: Application of Ultrasound. *Crystal Growth & Design, 24*(21), 9154-9162. [CrossRef]

[33] Sojoudi, H., Wang, M., Boscher, N. D., McKinley, G. H., & Gleason, K. K. (2016). Durable and scalable icephobic surfaces: similarities and distinctions from superhydrophobic surfaces. *Soft Matter, 12*(7), 1938–1963. [CrossRef]

[34] He, H., & Guo, Z. (2021). Superhydrophobic materials used for anti-icing Theory, application, and development. *Iscience, 24*(11), 103357. [CrossRef]

[35] Feng, X., Zhang, X., & Tian, G. (2022). Recent advances in bioinspired superhydrophobic ice-proof surfaces: challenges and prospects. *Nanoscale, 14*(16), 5960–5993. [CrossRef]

[36] Li, Q., & Guo, Z. (2018). Fundamentals of icing and common strategies for designing biomimetic anti-icing surfaces. *Journal of Materials Chemistry A, 6*(28), 13549-13581. [CrossRef]

[37] Chu, H., Xu, Q., Liu, Z., Xu, N., & Zhang, H. (2025). Eco-friendly photothermal superhydrophobic coatings: Recently advances in icephobic mechanisms, efficient photothermal conversion, and sustainable anti/de-icing technologies. *Advances in Colloid and Interface Science*, 103565. [CrossRef]

[38] Schutzius, T. M., Jung, S., Maitra, T., Eberle, P., Antonini, C., Stamatopoulos, C., & Poulikakos, D. (2015). Physics of icing and rational design of surfaces with extraordinary icephobicity. *Langmuir, 31*(17), 4807-4821. [CrossRef]

[39] Wang, L., Liu, M., Yadav, A., Wu, Y., & Zheng, H. (2023). A method for preparing and investigating anti-/de-icing surface by integration of laser-induced graphene (LIG) with a silica sol adhesive (SMP@ M-SiO2). *Surface and Coatings Technology, 474*, 130111. [CrossRef]

[40] Irajizad, P., Nazifi, S., & Ghasemi, H. (2019). Icephobic surfaces: Definition and figures of merit. *Advances in Colloid and Interface Science, 269*, 203–218. [CrossRef]

[41] Keshavarzi, S., Entezari, A., Maghsoudi, K., Momen, G., & Jafari, R. (2022). Ice nucleation on silicone rubber surfaces differing in roughness parameters and wettability: Experimental investigation and machine learning–based predictions. *Cold Regions Science and Technology, 203*, 103659. [CrossRef]

[42] Shen, Y., Tao, J., Tao, H., Chen, S., Pan, L., & Wang, T. (2015). Anti-icing Potential of Superhydrophobic Ti6Al4V Surfaces: Ice Nucleation and Growth. *Langmuir, 31*(39), 10799–10806. [CrossRef]

[43] Haechler, I., Ferru, N., Schnoering, G., Mitridis, E., Schutzius, T. M., & Poulikakos, D. (2023). Transparent sunlight-activated antifogging metamaterials. *Nature Nanotechnology, 18*(2), 137–144. [CrossRef]

[44] Tourkine, P., Le Merrer, M., & Quéré, D. (2009). Delayed freezing on water repellent materials. *Langmuir, 25*(13), 7214-7216. [CrossRef]

[45] Xing, M., Zhang, Z., Wang, Z., & Jing, D. (2024). Freezing process of water droplet on the cold plate surfaces with different wettability. *International Journal of Heat and Mass Transfer, 230*, 125773. [CrossRef]

[46] Liu, Y., Moevius, L., Xu, X., Qian, T., Yeomans, J. M., & Wang, Z. (2014). Pancake bouncing on superhydrophobic surfaces. *Nature Physics, 10*(7), 515–519. [CrossRef]

[47] Golovin, K., Dhyani, A., Thouless, M. D., & Tuteja, A. (2019). Low-interfacial toughness materials for effective large-scale deicing. *Science, 364*(6438), 371–375. [CrossRef]

[48] Hindmarsh, J. P., Russell, A. B., & Chen, X. D. (2003). Experimental and numerical analysis of the temperature transition of a suspended freezing water droplet. *International Journal of Heat and Mass Transfer, 46*(7), 1199-1213. [CrossRef]

[49] Li, A., Xu, Y., Qiu, C., Pang, J., Xu, Z., & He, Q. (2025). Dynamic de-icing mechanism analysis of propeller superhydrophobic surface droplets in flight environment. *Aerospace Science and Technology*, 110908. [CrossRef]

[50] Wong, T. S., Kang, S. H., Tang, S. K. Y., Smythe, E. J., Hatton, B. D., Grinthal, A., & Aizenberg, J. (2011). Bioinspired self-repairing slippery surfaces with pressure-stable omniphobicity. *Nature, 477*(7365), 443–447. [CrossRef]

[51] Zhang, P., Zhang, L., Chen, H., Dong, Z., & Zhang, D. (2017). Surfaces inspired by the Nepenthes peristome for unidirectional liquid transport. *Advanced Materials, 29*(45), 1702995. [CrossRef]

[52] Zhang, P., Zhang, L., Chen, H., Dong, Z., & Zhang, D. (2017). Surfaces inspired by the Nepenthes peristome for unidirectional liquid transport. *Advanced Materials, 29*(45), 1702995. [CrossRef]

[53] Yu, Z., Zhang, H., Yang, Y., Wang, B., & Guo, Z. (2025). Slippery liquid-infused porous surfaces (SLIPS) for anti-icing. *Materials Today, 88*, 906–932. [CrossRef]

[54] Liu, K., Zhang, Y., Li, B., & Chu, J. (2025). Durable slippery liquid-infused doubly reentrant surfaces for anti-fogging, anti-frosting and self-cleaning applications. *Surface & Coatings Technology, 514*, 132577. [CrossRef]

[55] Li, J., Lu, B., Cheng, Z., Cao, H., & An, X. (2024). Designs and recent progress of "pitcher plant effect" inspired ultra-slippery surfaces: A review. *Progress in Organic Coatings, 191*, 108460. [CrossRef]

[56] Cui, X., Ruan, Q., Zhuo, X., Xia, X., Hu, J., Fu, R., ... & Xu, H. (2023). Photothermal nanomaterials: a powerful light-to-heat converter. *Chemical Reviews, 123*(11), 6891-6952. [CrossRef]

[57] Liu, X., Mishra, D. D., Wang, X., Peng, H., & Hu, C. (2020). Towards highly efficient solar-driven interfacial evaporation for desalination. *Journal of Materials Chemistry A, 8*(35), 17907–17937. [CrossRef]

[58] Getaneh, S. A., Temam, A. G., Nwanya, A. C., Ejikeme, P. M., & Ezema, F. I. (2023). Advances in bioinspired superhydrophobic surface materials: A review on preparation, characterization and applications. *Hybrid Advances, 3*, 100077. [CrossRef]

[59] Xun, M., & Li, Z. (2025). Research Progress on Superhydrophobic Surface Preparation Methods and Mechanical Durability. *Recent Patents on Engineering, 19*(6), E150124225661. [CrossRef]

[60] Jung, S., Tiwari, M. K., Doan, N. V., & Poulikakos, D. (2012). Mechanism of supercooled droplet freezing on surfaces. *Nature Communications, 3*(1), 615. [CrossRef]

[61] Yun, Y. C., Ramachandraiah, K., & Hong, G. (2021). Effect of precooling conditions on the ice nucleation temperature and freezing characteristics of semisolid matrices. *Journal of Food Engineering, 291*, 110232. [CrossRef]

[62] PLOOSTER, M. N. (1968). Nucleation of Freezing in Supercooled Water by Cavitation. *Nature, 217*(5135), 1246–1247. [CrossRef]

[63] Wang, C., Zhang, H., Xu, Z., Hao, P., He, F., & Zhang, X. (2023). Whether contact time can evaluate the anti-icing properties of superhydrophobic surface-A research based on the MDPDE method. *International Journal of Heat and Mass Transfer, 215*, 124477. [CrossRef]

[64] Bird, J. C., Dhiman, R., Kwon, H., & Varanasi, K. K. (2013). Reducing the contact time of a bouncing drop. *Nature, 503*(7476), 385–388. [CrossRef]

[65] Guo, Q., Zheng, J., Fu, Z., Gao, H., & Wen, D. (2026). Water droplet impact-freezing behaviors on cold superhydrophobic cylindrical surfaces. *Experimental Thermal and Fluid Science, 171*, 111613. [CrossRef]

[66] Yang, C., Zeng, Q., Huang, J., & Guo, Z. (2022). Droplet manipulation on superhydrophobic surfaces based on external stimulation: A review. *Advances in Colloid and Interface Science, 306*, 102724. [CrossRef]

[67] Song, J., Gao, M., Zhao, C., Lu, Y., Huang, L., Liu, X., Carmalt, C. J., Deng, X., & Parkin, I. P. (2017). Large-Area Fabrication of Droplet Pancake Bouncing Surface and Control of Bouncing State. *ACS Nano, 11*(9), 9259–9267. [CrossRef]

[68] Zhai, Y., Liu, Q., Mohamed, M. E., Liu, F., Lv, S., Zhang, X., & Yang, X. (2024). Acid wet blasting method for fabricating superhydrophobic aluminum surface with micro-nano composite structures. *Applied Physics A, 130*(7), 464. [CrossRef]

[69] Ren, H., Hu, X., Wang, J., Li, N., & Chen, L. (2024). Vibration-Induced Pancake Bouncing of Impacting Droplets on Hydrophobic Surfaces. *Langmuir, 40*(42), 22338–22345. [CrossRef]

[70] Liu, Q., Yang, Y., Huang, M., Zhou, Y., Liu, Y., & Liang, X. (2015). Durability of a lubricant-infused Electrospray Silicon Rubber surface as an anti-icing coating. *Applied Surface Science, 346*, 68–76. [CrossRef]

[71] Wong, W. S. Y., Hegner, K. I., Donadei, V., Hauer, L., Naga, A., & Vollmer, D. (2020). Capillary Balancing: Designing Frost-Resistant Lubricant-Infused Surfaces. *Nano Letters, 20*(12), 8508–8515. [CrossRef]

[72] Yue, P., Zhang, Y., Zhang, S., Jia, J., Han, K., & Song, N. (2023). The critical role of interfacial Coulomb force in the orientation alignment behavior of lubricant molecules. *Tribology International, 187*, 108694. [CrossRef]

[73] Zhou, Y., Meng, Y., Cheng, Y., Guan, M., & Liu, X. (2024). High performances of cellulose nanocrystal based bicomponent supramolecular hydrogel lubricant. *Carbohydrate Polymers, 344*, 122542. [CrossRef]

[74] Wang, C., & Guo, Z. (2020). A comparison between superhydrophobic surfaces (SHS) and slippery liquid-infused porous surfaces (SLIPS) in application. *Nanoscale, 12*(44), 22398–22424. [CrossRef]

[75] Liang, J., Bian, H., Yang, Q., Fang, Y., Shan, C., Bai, X., ... & Chen, F. (2020). Femtosecond laser-patterned slippery surfaces on PET for liquid patterning and blood resistance. *Optics & Laser Technology, 132*, 106469. [CrossRef]

[76] Liu, G., Yang, J., Zhang, K., Yan, H., Yan, Y., Zheng, Y., ... & Chen, H. (2024). Nepenthes alata inspired anti-sticking surface via nanosecond laser fabrication. *Chemical Engineering Journal, 483*, 149192. [CrossRef]

[77] Ponomarev, V. A., Shvindina, N. V., Permyakova, E. S., Slukin, P. V., Ignatov, S. G., Sirota, B., ... & Shtansky, D. V. (2019). Structure and antibacterial properties of Ag-doped micropattern surfaces produced by

photolithography method. *Colloids and Surfaces B: Biointerfaces, 173*, 719-724. [CrossRef]

[78] Xiang, T., Liu, J., Liu, Q., Wei, F., Lv, Z., Yang, Y., ... & Xu, G. (2021). Self-healing solid slippery surface with porous structure and enhanced corrosion resistance. *Chemical Engineering Journal, 417*, 128083. [CrossRef]

[79] Zhu, X., Yao, Y., Li, J., Mu, L., Liu, Q., Sun, C. L., ... & Qu, M. (2024). A mechanically durable slippery liquid-infused porous surface based on distinctive 'jaboticaba-like'TiO2/sepiolite nanocomposites with superior hot water repellency and anti-corrosion for protecting various substrates. *Chemical Engineering Journal, 481*, 148667. [CrossRef]

[80] Okada, I., & Shiratori, S. (2014). High-transparency, self-standable Gel-SLIPS fabricated by a facile nanoscale phase separation. *ACS Applied Materials & Interfaces, 6*(3), 1502–1508. [CrossRef]

[81] Li, S., Zhao, F., Bai, Y., Ye, Z., Feng, Z., Liu, X., Gao, S., Pang, X., Sun, M., Zhang, J., Dong, A., Wang, W., & Huang, P. (2022). Slippery liquid-infused microphase separation surface enables highly robust anti-fouling, anti-corrosion, anti-icing and anti-scaling coating on diverse substrates. *Chemical Engineering Journal, 431*, 133945. [CrossRef]

[82] Bollmann, W., & Spreadborough, J. (1960). Action of graphite as a lubricant. *Nature, 186*(4718), 29–30. [CrossRef]

[83] Ahuja, A., & Rastogi, V. K. (2023). Spray coating of edible insect waxes for liquid food packaging. *Applied Surface Science, 624*, 157150. [CrossRef]

[84] Yang, C., & Guo, Z. (2025). Multifunctional aluminum alloy slippery liquid-infused surface with porous and boehmite nanoflower structure. *Journal of Colloid and Interface Science, 683*, 421–434. [CrossRef]

[85] Golovin, K., Kobaku, S. P., Lee, D. H., DiLoreto, E. T., Mabry, J. M., & Tuteja, A. (2016). Designing durable icephobic surfaces. *Science advances, 2*(3), e1501496. [CrossRef]

[86] Sun, X., Damle, V. G., Liu, S., & Rykaczewski, K. (2015). Bioinspired stimuli-responsive and antifreeze-secreting anti-icing coatings. *Advanced Materials Interfaces, 2*(5), 1400479. [CrossRef]

[87] Liu, Z., Hu, J., & Jiang, G. (2022). Superhydrophobic and photothermal deicing composite coating with self-healing and anti-corrosion for anti-icing applications. *Surface and Coatings Technology, 444*, 128668. [CrossRef]

[88] Zhang, Y., Fan, X., Li, X., Zhang, Z., Zhang, Y., Chen, Z., Ge, S., Wang, Y., & Zhu, M. (2024). Micro-structure design of black ceramic composite surface towards photothermal superhydrophobic anti-icing. *Chemical Engineering Journal, 498*, 155101. [CrossRef]

[89] Luo, W., Zou, M., Luo, L., Ma, Y., Chen, W., Hu, X., Li, Q., & Jiang, X. (2024). Efficient enhancement of photothermal conversion of polymer-coated phase change materials based on reduced graphene oxide and polyethylene glycol. *Journal of Energy Storage, 78*, 109950. [CrossRef]

[90] Zhou, M., Cui, C., Chen, Y., Huang, Q., Lian, Y., Chen, H., Zhang, Y., Qi, X., & Chen, Z. (2025). A photothermal superhydrophobic sponge based on carbon nanotubes with environmental tolerance, flame-retardant, antibacterial, and high oil-absorption properties. *Chemical Engineering Science, 316*, 121997. [CrossRef]

[91] Xue, Q., Wu, W., Wu, J., Zhang, Y., Gao, X., Lv, Z., Lei, Y., & Huang, Y. (2024). Nano-Fe3O4/chitosan-based superhydrophobic coatings with magnetic oil-water separation and photothermal conversion properties. *Colloids and Surfaces a-Physicochemical and Engineering Aspects, 689*, 133698. [CrossRef]

[92] Li, Y., Sun, H., Li, X., Lin, B., Liu, H., & Liang, C. (2026). Charge transfer and thermal conduction mechanisms in superhydrophobic Gr-TiO_2 photothermal coatings for high-efficiency deicing. *Progress in Organic Coatings, 211*, 109788. [CrossRef]

[93] Zhang, G., Liang, C., Li, A., Lu, B., Li, X., Lin, B., & Gao, S. (2026). Synergistic photothermal and superhydrophobic effects: design and molecular mechanism of anti-icing coatings based on MWCNTs-COOH/TiN@HDTMS. *Applied Surface Science, 720*, 165150. [CrossRef]

[94] Li, Q., Yang, S., Ying, Y., Liu, Y., Wen, R., Miljkovic, N., & Ma, X. (2025). Scalable Photothermal Superhydrophobic Deicing Coating with Mechanochemical-Thermal Robustness. *ACS Applied Materials & Interfaces, 17*(38), 54302–54313. [CrossRef]

[95] Wu, M., Zhang, Y., He, Z., Ding, H., & Wu, W. (2026). Robust durable photothermal superhydrophobic coatings based on mussel-inspired adhesion chemistry for efficient anti-/de-icing. *Colloids and Surfaces a-Physicochemical and Engineering Aspects, 728*, 138502. [CrossRef]

[96] Hou, M., Jiang, Z., Sun, W., Chen, Z., Chu, F., & Lai, N. (2024). Efficient Photothermal Anti-/Deicing Enabled by 3D Cu2-xS Encapsulated Phase Change Materials Mixed Superhydrophobic Coatings. *Advanced Materials, 36*(3), 2310312. [CrossRef]

[97] Li, D., Zhang, Y., Gao, S., Wang, Z., & Bai, G. (2025). Transparent Anti-Icing Coating via Synergistic Nanoscale Interfacial Engineering and Spectral-Selective Photothermy. *Advanced Functional Materials*, e13944. [CrossRef]

[98] Yao, F., Wei, J., Xu, Y., Tu, H., Huang, M., Tang, Q., Zhao, S., & Wang, J. (2025). Light-trapping superhydrophobic coatings with switchable wettability to solve low-temperature anti-icing/deicing and high-temperature overheating problems on surfaces. *Journal of Colloid and Interface Science, 699*, 138275. [CrossRef]

[99] Yu, G., & Jiang, G. (2024). Fabrication of a superhydrophobic surface with photothermal electrical conversion performance for anti-icing. *Surfaces and Interfaces, 46*, 104089. [CrossRef]

[100] Pang, J., Qiu, W., Meng, Q., Zhou, J., Wang, X., & Yue, Y. (2025). Design and Research of an Aircraft Ice Control System Based on Multilayer Functional Film. *Advanced Engineering Materials, 27*(7), 2402352. [CrossRef]

[101] Chu, F., Hu, Z., Feng, Y., Lai, N., Wu, X., & Wang, R. (2024). Advanced Anti-Icing Strategies and Technologies by Macrostructured Photothermal Storage Superhydrophobic Surfaces. *Advanced Materials, 36*(31), 2402897. [CrossRef]

[102] Fu, D., Zheng, H., Sheng, W., Hao, X., Zhang, X., Chang, S., & Song, M. (2024). An experimental study on the influence of humidity on ice adhesion strength on superhydrophobic surfaces with microstructures. *Applied Thermal Engineering, 244*, 122732. [CrossRef]

[103] Bharathidasan, T., Kumar, S. V., Bobji, M. S., Chakradhar, R. P. S., & Basu, B. J. (2014). Effect of wettability and surface roughness on ice-adhesion strength of hydrophilic, hydrophobic and superhydrophobic surfaces. *Applied Surface Science, 314*, 241–250. [CrossRef]

[104] Boinovich, L. B., Emelyanenko, K. A., & Emelyanenko, A. M. (2022). Superhydrophobic versus SLIPS: Temperature dependence and the stability of ice adhesion strength. *Journal of Colloid and Interface Science, 606*, 556–566. [CrossRef]

[105] Wu, Y., Dong, L., Shu, X., Chen, L., Zhang, Y., & Ran, Q. (2025). Fluorine-free photothermal superhydrophobic fabrics with self-healing and ice-resistant properties for cold-environment protection. *Materials & Design, 256*, 114262. [CrossRef]



Jingxian Yang received the PhD. degree in materials science and engineering from southeast University, Nanjing 211189, CN, in 2025. (Email: jingxianyang@kust.edu.cn)



Zhangyu Wu received the PhD. degree in Civil Engineering from Nanjing University of Aeronautics and Astronautics, Nanjing 210016, CN, in 2023. (Email: wuzy@seu.edu.cn)



BinBin He received the PhD. degree in Chemical Engineering and Technology from Kunming University of Science and Technology, Kunming 650500, CN, in 2023. He was selected as a technological innovation talent in Yunnan Province, recognized as an outstanding professional and technical talent for his significant contributions (second-class) in Yunnan, and honored as a model worker in Kunming City. (Email: Kust2024hb@163.com)



Wei She received the PhD. degree in materials science and engineering from southeast University, Nanjing 211189, CN, in 2014. He serves as an Associate Editor for the Journal of Building Engineering, a top-ranked journal in the JCR (Journal Citation Reports) 1st quartile, and was selected for Stanford University's Global Top 2% Scientists List. (Email: weishe@seu.edu.cn)